

1 Long-term change in the ~~contributions of various source~~ 2 regions contribution to surface ozone over Japan

3
4 **Tatsuya Nagashima¹, Kengo Sudo^{2,3}, Hajime Akimoto¹, Junichi Kurokawa⁴, and**
5 **Toshimasa Ohara¹**

6 ¹National Institute for Environmental Studies, Tsukuba, Japan

7 ²Graduate School of Environmental Studies, Nagoya University, Nagoya, Japan

8 ³Frontier Research Center for Global Change, Yokohama, Japan

9 ⁴Asia Center for Air Pollution Research, Niigata, Japan

10 *Correspondence to:* T. Nagashima (nagashima.tatsuya@nies.go.jp)

11 12 **Abstract**

13 The relative contributions of various source regions to the long-term (1980–2005) increasing
14 trend in surface ozone (O₃) over Japan were estimated by a series of tracer-tagging
15 simulations using a global chemical transport model. The model well simulated the observed
16 increasing trend of surface O₃ including its seasonal variation and geographical features in
17 Japan and demonstrated the relative roles of different source regions in forming this trend.
18 Most of the simulated increasing trend of surface O₃ over Japan (~97 %) was explained as the
19 sum of trends in contributions of different regions to photochemical O₃ production. The
20 increasing trend in O₃ produced in China accounted for 36 % of the total increasing trend and
21 those in the other northeast Asian regions (the Korean Peninsula, coastal regions in East Asia,
22 and Japan) each accounted for about 12–15 %. Furthermore, the contributions of O₃ created in
23 the entire free troposphere and in West, South, and Southeast Asian regions also increased;
24 and their increasing trends accounted for 16 and 7 % of the total trend, respectively. The
25 impact of interannual variations in climate, in methane concentration, and in emission of O₃
26 precursors from different source regions on the relative contributions of O₃ created in each
27 region estimated above was also investigated. The variation of climate and the increase in
28 methane concentration together caused the increase of photochemical O₃ production in several
29 regions, and represented about 19 % of the total increasing trend of surface O₃ over Japan.
30 The increase in emission of O₃ precursors in China caused an increase of photochemical O₃
31 production not only in China itself but also in the other northeast Asian regions and accounted
32 for about 46 % of the total increase in surface O₃ over Japan. Similarly, the relative impact of
33 O₃ precursor emission changes in the Korean Peninsula and Japan were estimated as about 16
34 and 4 % of the total increasing trend, respectively. The O₃ precursor emission change in
35 regions other than northeast Asia caused increases in surface O₃ over Japan mainly through
36 increasing photochemical O₃ production in West, South, and Southeast Asia and the free
37 troposphere, and accounted for about 16 % of the total.

38 1 Introduction

39 Tropospheric ozone (O_3) ~~plays multiple roles in the atmosphere. O_3 itself~~ is an oxidant and
40 photodissociates to generate the hydroxyl radical which strongly oxidizes many atmospheric
41 compounds including various air pollutants and thus removes them from the atmosphere. In
42 contrast, high levels of O_3 are a major air pollutant due to adverse effects on human health,
43 natural vegetation, and agricultural produce (Wang and Mauzerall, 2004; Mauzerall et al.,
44 2005; US EPA, 2006; Silva et al., 2013). Moreover, tropospheric O_3 is a major greenhouse
45 gas in the atmosphere, and reduction of its amount was recently recognized as an effective
46 measure to mitigate near-term climate change (UNEP and WMO, 2011; Shindell et al., 2012).
47 Therefore, the spatial and temporal variations in tropospheric O_3 have been always a matter of
48 scientific and public concern.

49 ~~An increasing trend in tropospheric O_3 concentration has been observed during recent~~
50 ~~decades at many locations in East Asia including Taiwan (Chou et al., 2006; Chang and Lee;~~
51 ~~2007; Li et al., 2010; Lin et al., 2010), mainland China (Lu and Wang, 2006; Ding et al.,~~
52 ~~2008; Xu et al., 2008; Wang et al., 2009; Zhang et al., 2014), and South Korea (Susaya et al.,~~
53 ~~2013; Lee et al., 2014; Seo et al., 2014). The increase rates of O_3 in those East Asian regions~~
54 ~~significantly vary depending on location and season in the range of about 0.3–3 ppbv/yr;~~
55 ~~however, the increases are generally larger than the trends in tropospheric O_3 for other regions~~
56 ~~in the world (Cooper et al., 2014). Japan is no exception experienced a rapid industrialization~~
57 ~~ahead of other Asian countries, with and an increasing trend has been found in various~~
58 observations of O_3 over the past approximately 40 years. Routine ozonesonde measurements
59 since 1970 at three Japanese sites of Sapporo (43° N), Tsukuba (36° N), and Kagoshima (32°
60 N) showed an increasing trend of O_3 concentration in the lowermost troposphere up to about
61 1990 and relatively stable thereafter, with largest increase near the ground and discernible
62 about 300 hPa height and below (Logan et al., 1999; Oltmans et al., 2006). With an air mass
63 classification method based on backward air trajectories, Naja and Akimoto (2004) showed
64 that a significant amount of the air masses reaching these ozonesonde sites in Japan spend
65 substantial time over polluted regions in East Asia. The O_3 levels in these regionally polluted
66 air masses increased from the 1970s to the 1990s, mainly due to large increases in nitrogen
67 oxide ($NO_x = NO + NO_2$) emissions over China in the 1990s. Oltmans et al. (2013) analyzed a
68 rather short period of data (1991–2010) obtained at the Ryori (39° N) surface site in north-
69 eastern Japan and showed an increase into the mid-1990s followed by relatively little change.
70 Other ground-based observations at a mountain site (Mt. Happo; 43° N, 1850 m asl) and three
71 sites in the marine boundary layer along the west coast of Japan [Rishiri (45° N), Tappi (41°
72 N), and Sado (38° N)], where few sources of pollutants exist nearby, obtained under the
73 monitoring network of EANET (the Acid Deposition Monitoring Network in East Asia) also
74 showed increasing trends of O_3 concentrations at least until the mid-2000s (Tanimoto, 2009;
75 Tanimoto et al., 2009; Parrish et al., 2012). During the recent decades, an increasing trend in
76 tropospheric O_3 has also been observed at many locations in East Asia including Taiwan
77 (Chou et al., 2006; Chang and Lee; 2007; Li et al., 2010; Lin et al., 2010), mainland China
78 (Lu and Wang, 2006; Ding et al., 2008; Xu et al., 2008; Wang et al., 2009; Zhang et al., 2014),
79 and South Korea (Susaya et al., 2013; Lee et al., 2014; Seo et al., 2014). The increase rates of
80 O_3 in those East Asian regions significantly vary depending on location and season in the
81 range of about 0.3–3 ppbv/yr; however, the increases are generally larger than the trends in
82 tropospheric O_3 for other regions in the world (Cooper et al., 2014).

83 In addition Japan, analysis of long-term observations by the ambient air quality monitoring
84 network mainly established in urban–suburban regions ~~in Japan~~ also showed continuous
85 increases of surface O_3 from the mid-1980s until the present (Ohara and Sakata, 2003; Ohara

86 et al., 2008; Kurokawa et al., 2009; MOE Japan, 2013; Wakamatsu et al., 2013; Akimoto et
87 al., 2015). And the consequent high violation rate of national ambient air quality standard
88 (AAQS) for surface O₃ (hourly mean concentration of 60 ppbv) has been the persistent issue
89 in environmental administration for a long time, therefore, there is an urgent need to study the
90 reason for the increasing trend and examine the countermeasures. However, One clue is that
91 the simultaneous observations of O₃ precursors such as NO_x and non-methane hydrocarbons
92 (NMHCs) by this monitoring network revealed their decreasing trends in the same period
93 (MOE Japan, 2013), which seemed inconsistent with the increasing trend of O₃ over Japan.
94 These observed features of O₃-related atmospheric species in Japan suggest that there should
95 be an influence of transboundary transport from outside of Japan on the recent increasing
96 trend in O₃. The influence of transboundary transport on surface O₃ in East Asia was
97 examined in several studies (Sudo and Akimoto, 2007; Li et al., 2008; Nagashima et al., 2010;
98 Wang et al., 2011). Nagashima et al. (2010) demonstrated that the O₃ transported from outside
99 of Japan accounted for more than 70 % of surface O₃ over Japan in the cold season (October–
100 March) during 2000–2005, and most was attributable to O₃ from distant sources outside East
101 Asia and from the stratosphere. In the warm season (April–September), the contribution of
102 domestically created O₃ in Japan to surface O₃ over Japan increased significantly (about 20–
103 40 %), the short range intra-regional transport of O₃ from other parts of East Asia still
104 contributed about 25 %, and long range inter-regional transport of O₃ from outside East Asia
105 and the stratosphere particularly in spring could account for about half of surface O₃ over
106 Japan.

107 Therefore, the influence of O₃ from source regions outside and inside East Asia and the
108 stratosphere should be considered to explain the cause of the increasing trend in surface O₃
109 over Japan. The rapid increase in O₃ precursor emissions in East Asia in recent decades
110 (Ohara et al., 2007; Kurokawa et al., 2013) was demonstrated as a major cause of the
111 increasing trend of springtime O₃ over Japan by comparing regional chemical transport model
112 (CTM) simulations of recent decades with and without the East Asian O₃ precursor emission
113 increases during the period (Kurokawa et al., 2009; Tanimoto et al., 2009). However, they
114 only showed the springtime O₃ case and it was unclear whether the relationship held in other
115 seasons. Moreover, the relative contributions of individual countries or regions in East Asia
116 have not been well examined, particularly concerning increased surface O₃ over Japan.

117 Here, we investigated the cause of the continuous increase in surface O₃ over Japan reported
118 in the above literature, focusing on the relative contributions of various source regions over
119 the globe, particularly the contributions of individual regions in East Asia, with a long-term
120 simulation of a global CTM using the tagged tracer method. Using the same model and
121 method, Nagashima et al. (2010) showed such relative contributions of regions inside and
122 outside East Asia on surface O₃ over Japan as average values for the early 2000s. The current
123 study investigated the temporal evolution of the relative contributions of each region for the
124 26 years of 1980–2005.

125

126 **2 Methods**

127 **2.1 Model description**

128 In this study, we employed a chemistry climate model (CCM), CHASER (Sudo et al., 2002),
129 developed for the atmospheric chemistry research in the troposphere. The basic setting of the
130 model was almost identical to that used by Nagashima et al. (2010). However, the horizontal
131 resolution was modified from T63 (about 1.9° by 1.9° grid spacing in longitude and latitude)

132 to T42 (about 2.8° by 2.8°), because longer simulation period was necessary than in the
133 previous study, and so the cost of computation was reduced in the present study by selecting
134 lower horizontal resolution. There were 32 vertical layers with the top layer set at
135 approximately 40 km altitude. A detailed tropospheric photochemistry consisted of 113
136 chemical reactions and 27 photodissociation involving O₃, HO_x, NO_x, methane (CH₄), CO and
137 NMHCs calculated the temporal evolution in the concentrations of 53 chemical species. ~~The
138 gas and liquid phase oxidation of sulfur dioxide (SO₂) and dimethyl sulfide to form the sulfate
139 aerosol was also included in the model.~~ The concentrations of O₃ and some nitrogen
140 compounds (NO_x, HNO₃, and N₂O₅) above the tropopause that should affect tropospheric
141 chemistry were assimilated into the monthly mean output data of stratospheric CCM, because
142 the version of CHASER used was unable to calculate several chemical processes, such as
143 halogen-related chemical reactions, which are indispensable for realistic representation of
144 such chemical compounds in the stratosphere. ~~For the transport of chemical species, a semi-
145 Lagrangian advective transport scheme (Lin and Rood, 1996; van Leer, 1997) and vertical
146 convective transport associated with cumulus convection process were considered.~~ The model
147 also included dry and wet deposition of chemical species.

148 In this study, we conducted tracer-tagging simulation by using two different setups (full-
149 chemistry and tracer-transport setups) of CHASER. The full-chemistry setup calculated the
150 actual temporal change in the concentration of chemical species through the abovementioned
151 chemical and physical processes and outputted the chemical production and loss tendencies of
152 O₃ and related species. Then, the tracer-transport setup used the outputted chemical
153 tendencies to calculate the temporal change in the concentration of hypothetical O₃ tracers. In
154 the following subsection, the calculation procedure is briefly described.

155

156 **2.2 Outline of the numerical simulations**

157 **2.2.1 Forcings for long-term simulation**

158 Long-term simulation was performed for the period 1980–2005. The end of simulation
159 period (2005) was determined mainly due to the temporal coverage of the Asian emission data
160 described below, however, this period sufficiently covered the years reported to have
161 increasing trend in surface O₃ over Japan in the previous literatures. To drive the physical
162 properties of the model for this 26-year period, the temperature and horizontal wind velocities
163 in the model were assimilated into the National Center for Environmental Prediction/National
164 Center of Atmospheric Research (NCEP/NCAR) 6-hour reanalysis data (Kalnay et al., 1996)
165 of the corresponding year, and sea surface temperature and sea ice data of the Hadley Centre's
166 Sea Ice and Sea Surface Temperature (HadISST) data set (Rayner et al., 2003) were used in
167 the model.

168 The monthly mean stratospheric O₃ data of Akiyoshi et al. (2009) was used for the
169 assimilation above the tropopause for this period. These data were the output of a
170 stratospheric CCM simulation according to the hindcasting scenario for 1980–2004 (REF1
171 scenario) of the CCM validation activity (CCMVal) (Eyring et al., 2005), and included an
172 interannual variation (IAV) associated with the 11-year solar cycle and large declines after
173 1982 and 1991 due to the El Chichon and Pinatubo eruptions, respectively, in addition to a
174 continuous decreasing trend during the whole period. Although the simulated declines of
175 stratospheric O₃ due to the two large volcanic eruptions were somewhat overestimated, the
176 simulated IAVs in stratospheric O₃ reasonably well represented those observed with a total

177 ozone mapping spectrometer (TOMS) from satellites (Akiyoshi et al., 2009). Incidentally, the
178 stratospheric O₃ data of 2004 were used for 2005.

179 The long-term variation of the emissions of O₃ precursors (NO_x, CO, and NMHCs) ~~and SO₂~~
180 were taken from multiple emission inventories. For anthropogenic emissions in Asia, the
181 Regional Emission inventory in ASia (REAS ver.1.2) (Ohara et al., 2007) was used for each
182 year in the whole simulation period (1980–2005); ~~the REAS emission data were available for~~
183 ~~each year in the period.~~ Kurokawa et al. (2009) used these emission data with a regional air
184 quality model representing well the interannual variability of surface O₃ over Japan for
185 similar period (1981–2005) to the present study. For anthropogenic emissions outside Asia, a
186 combination of three versions of EDGAR (Emission Database for Global Atmospheric
187 Research) emission data was used: EDGAR-HYDE (Van Aardenne et al., 2001) for 1980 and
188 1990; EDGAR v3.2 (Olivier and Berdowski, 2001) for 1990 and 1995; and EDGAR v3.2 Fast
189 Track 2000 (FT2000) (Olivier and Berdowski, 2001) for 2000. Because several emission
190 sectors considered in EDGAR v3.2 were not considered in EDGAR-HYDE, the emissions for
191 1990 in EDGAR-HYDE were generally smaller than in EDGAR v3.2. Therefore, we used
192 EDGAR v3.2 data for 1990, and also scaled them to estimate emission data for 1980 rather
193 than simply using EDGAR-HYDE data for 1980. For that, we scaled EDGAR v3.2 data for
194 1990 so that the ratio (r) of the difference between 1980 (f_1) and 1990 data (f_2) and their
195 average in EDGAR-HYDE [i.e., $r = (f_2 - f_1)/(f_1 + f_2)/2$] equaled the corresponding ratio (R)
196 calculated from 1990 data in EDGAR v3.2 (F_2) and 1980 data scaled from it (F_1) [i.e., $R = (F_2$
197 $- F_1)/(F_1 + F_2)/2$]. We calculated F_1 from the known values of f_1 , f_2 , and F_2 using the equation
198 $r = R$. Since EDGAR emission data were not available for each year but for every 10 or 5
199 years in the simulation period, the emissions for intermediate years were interpolated, and
200 FT2000 data used for years after 2000. The vegetation fire emission data developed in the
201 REanalysis of the TROpospheric chemical composition over the past 40 years project
202 (RETRO) (Schultz et al., 2008) were used for O₃ precursor emissions from biomass burning
203 ~~for the whole land area. RETRO data were available~~ for each year until 2000 in the simulation
204 period, and data for 2000 were used for years after 2000. Historical transition of the
205 atmospheric concentrations of carbon dioxide, nitrous oxide (~~N₂O~~), and CH₄ were prescribed
206 with those used in Nozawa et al. (2005), which were somewhat old estimations of the
207 historical evolution in greenhouse gas concentrations, but not much different from recent
208 estimations such as for the Representative Concentration Pathways (RCPs) (Meinshausen et
209 al., 2011). The difference in the concentrations between both estimations were generally
210 within a couple of percent in the simulation period.

211 The linear trends of NO_x and NMVOC annual emissions used in this study in the simulation
212 period of 1980–2005 are shown in Fig. 1. The long-term trends of emissions of both species
213 showed generally similar geographical features to each other; large decrease trends in central
214 Europe, Scandinavia, western Russia, and Kazakhstan, whereas there were widely spread
215 increasing emissions in West, South, Southeast, and East Asia, almost all Africa and Central
216 and South America except for inland Brazil. In North America, NO_x emission generally
217 decreased in the simulation period except for the west coast and New England area of the
218 USA, but that of NMVOC mostly increased with a few patchy exceptions. The trends of NO_x
219 and NMVOC emissions mentioned above were mainly due to the change in anthropogenic
220 emissions, while the change in biomass burning emissions led to a discernible trend in several
221 regions such as inland Brazil and the south of Sahel.

222 The long-term evolution of annual emissions of NO_x and NMVOC over several source areas
223 in the Northern Hemisphere is shown in Fig. 2. Because the emission data were the
224 combination of three different datasets outside Asia, there were somewhat discontinuous

225 changes at the joint years (1990 and 1995) in European and North American emissions. The
226 emissions of NO_x and NMVOC over Europe had peaks around 1990 and generally decreased
227 afterward. Over North America, both species showed small long-term trends: slight decreases
228 in NO_x and slight increases in NMVOC emissions. The emissions of both species over China
229 greatly increased during the whole period. The NO_x emissions were about 4.0 times larger in
230 2005 than 1980 and correspondingly NMVOC was 2.5 times larger, which made emissions of
231 both species for China equal to or even surpassing those for Europe or North America in 2005.
232 The emissions of both species over the Korean Peninsula increased approximately 2.8 times
233 during this period. However, those over Japan showed no such increase: NO_x emission
234 decreased until 1995 and thereafter remained stable, whereas NMVOC emissions went up
235 until 1995 and then slightly decreased.

236 **2.2.2 Tracer tagging**

237 We conducted a 26-year simulation using the full-chemistry setup of CHASER with all the
238 forcings mentioned above, followed by another 26-year simulation with the tracer-transport
239 setup of CHASER which calculated the concentration of hypothetical O₃ tracers, each tagged
240 with a particular region in the model domain. The procedure to tag a tracer with each region
241 in the second simulation was the same as used by Nagashima et al. (2010) and a brief
242 description follows. In the second simulation, the transport and dry deposition of each O₃
243 tracer were calculated same as in the first simulation, however the chemical development of
244 tracers was calculated using the chemical production (P) and loss frequencies (L) of the
245 extended odd oxygen family [O_x = O₃ + O + O(¹D) + NO₂ + 2NO₃ + 3N₂O₅ + PANs + HNO₃
246 + other nitrates] calculated and archived in the first simulation. In the first simulation, 3D
247 fields of P and L were outputted every 6 hours. Each O₃ tracer could be lost chemically
248 everywhere in the model domain at the frequency of L, but could be chemically produced
249 only inside its tagged region. In the stratosphere ~~over the tropopause defined by the lapse rate,~~
250 the concentration of O₃ tracer tagged with the stratosphere was assimilated into the same
251 stratospheric O₃ data as used in the first simulation, but the concentration of the tracers tagged
252 with the region in the troposphere were all set to zero. The calculated concentration of each
253 tagged O₃ tracer at a given location represents the contribution of O₃ produced in each source
254 region and transported to that location.

255 ~~The horizontal and vertical separation of the model domain for the tracer tagging was also~~
256 ~~the same as used by Nagashima et al. (2010).~~ The troposphere in the model domain was
257 horizontally separated into 22 regions and each horizontal region was further separated
258 vertically between the free troposphere (FT) and the planetary boundary layer (PBL). The
259 stratosphere was considered one separate source region, that is, the model domain was
260 separated into 45 source regions. The 22 regions for horizontal separation are shown in Fig. 1
261 and each region was assigned a three-letter code (e.g., AMN for North America) which is
262 used in the following sections. For the vertical separation of the source regions in the
263 troposphere, the PBL was defined as the lowest six layers in the model (surface to about 750
264 hPa), based on the observed and modeled vertical profiles of O₃ production.

265 The long-term tracer-tagging simulation allowed estimation of the long-term variations in
266 contributions of each source region to the O₃ concentration at given receptor locations. This is
267 important information to explain the cause of the reported increasing trend in surface O₃ over
268 East Asia. However, it should be noted that the tracer-tagging simulation calculates the
269 amount of O₃ in a receptor location that was produced chemically in each source region from
270 O₃ precursors emitted both from the source region and adjacent source regions. Thus, the
271 contribution of a source region estimated in tracer-tagging simulation should not be fully

272 attributed to emissions of O₃ precursors in that source region. Emission sensitivity simulation
273 is another method of estimating the portion of O₃ fully attributable to a change in O₃ precursor
274 emissions in a source region, and takes the difference of simulated O₃ between two model
275 runs with and without perturbed O₃ precursor emissions in that source region. The resulting
276 estimations of source contributions by the two methods can differ; however, the differences
277 have not yet been well quantified. Li et al. (2008) reported that the difference between the two
278 methods could be as much as 30 % in source apportionment estimation for one location and
279 time (i.e., Mt. Tai in central eastern China in June 2006). Wang et al. (2011) found somewhat
280 larger differences in the contributions of China to domestic O₃ concentration between the two
281 methods for each month of the year, but no discussions were made for O₃ over Japan.

282 Nevertheless, we employed the tracer-tagging simulation to study the cause of reported long-
283 term change in surface O₃ over Japan mainly due to its computational efficiency. Thus, the
284 results should be carefully interpreted in terms of the difference between the source regions of
285 chemical O₃ production and those of O₃ precursor emissions. The computational efficiency
286 resulting from the tracer-tagging approach and relatively coarse horizontal resolution enabled
287 us to make several sensitivity simulations with the different combination of forcings for long-
288 term simulation. In the following sections, the simulation with the full set of long-term
289 forcings described above, hereinafter referred to as “standard” simulation, is initially analyzed.
290 This is then further interpreted using the results of sensitivity simulations; the specific settings
291 of sensitivity simulations are also described.

292

293 **3 Results and discussion**

294 **3.1 Long-term evolution of surface O₃ over Japan**

295 Nagashima et al. (2010) validated how well CHASER can reproduce the observed features
296 of surface O₃ concentrations by comparing the simulated surface O₃ concentrations with
297 observations taken during 2000–2005 at several sites mainly in rural areas in the Northern
298 Hemisphere, and CHASER successfully simulated the annual variation of surface O₃ in a
299 variety of regions. In this study, the horizontal resolution of the model differed from that used
300 in Nagashima et al. (2010); however, the model well represented the observed concentrations
301 and seasonal evolutions of surface O₃ (Fig. S1 and Table S1 in the Supplement). The surface
302 O₃ over Japan has been observed at ambient air quality monitoring stations since the early
303 1970s ~~when severe air pollution occurred in industrial or urban areas~~. The monitoring data
304 have been compiled by the Atmospheric Environmental Regional Observation System
305 (AEROS). ~~The number of stations increased since the launch of the system and, for the period~~
306 ~~of simulation (1980–2005), a~~ about 1000 monitoring stations widely distributed throughout
307 Japan except in the southern islands could be used for validation of the model results. The
308 monitoring data of AEROS have been used to examine the long-term variation of surface O₃
309 over Japan in several studies and showed significant increasing trends (Ohara and Sakata,
310 2003; Ohara et al., 2008; Kurokawa et al., 2009; Akimoto et al., 2015). We validated the
311 simulated surface O₃ over Japan with the AEROS data in terms of the long-term variation in
312 the following.

313 For the validation, the monitoring sites selected had continuously observed the surface O₃
314 during the simulation period (1980–2005). To ensure continuity of sites, we selected
315 monitoring sites with annual mean surface O₃ available for every year in the simulation period.
316 The annual mean data at a monitoring site was calculated as the average of monthly means
317 when available for more than 9 months, the monthly mean was calculated from daily means

318 when available for over 19 days per month, and the daily mean was calculated from hourly
319 means when available for more than 19 hours per day. There were 339 sites, located mainly in
320 populated areas of Japan except in the northernmost island (Hokkaido) and southern islands
321 (Nansei Islands). We first calculated the annual mean surface O₃ ~~from the observed hourly~~
322 ~~data at each monitoring site as described above~~, and then the annual means of all sites were
323 averaged to calculate the observed annual mean surface O₃ over Japan. The simulated annual
324 mean surface O₃ over Japan was calculated as the average of annual means of the model grids,
325 which included the locations of monitoring sites selected for the validation. ~~Therefore, the~~
326 ~~model grids including Hokkaido or Nansei Islands were not used to calculate the simulated~~
327 ~~annual mean.~~ The temporal variations of observed and simulated annual mean surface O₃
328 anomalies during 1980–2005 averaged over Japan are shown in Fig. 3. During the period, the
329 observed annual mean surface O₃ over Japan showed a clear increasing trend with a linear
330 increase of about 2.70 ppbv/decade, which was significant at the 5 % risk level. The simulated
331 annual mean surface O₃ over Japan also showed a significant increasing trend with a rate of
332 about 2.58 ppbv/decade, which corresponded well to the observed increase in surface O₃ over
333 Japan. The value of the linear increasing trend and the observed features of IAVs-long-term
334 variation in surface O₃ over Japan – such as a rapid increase from the mid-1980s to the mid-
335 1990s followed by a stagnation of increase for about 7–8 years and a further increase in the
336 past several years – were reasonably well captured by the model.

337 The model also well represented the longitudinal differences in the long-term trend of
338 surface O₃ in Japan. Figure 4 shows the maps of linear trends of annual mean surface O₃
339 during 1980–2005 calculated from the model simulations and observations at AEROS
340 monitoring sites as selected for Fig. 3. The simulated annual mean surface O₃ showed an
341 increasing trend in the whole area including all of Japan and the Korean Peninsula (Fig. 4a).
342 The simulated increasing trend of annual mean surface O₃ well exceeded 2.0 ppbv/decade in
343 wide areas of Japan except for Hokkaido, and tended to be greater toward western Japan,
344 which is nearer to the Asian continent. However, the increasing trends of observed annual
345 mean surface O₃ at each monitoring site (Fig. 4b) differed greatly from each other even in
346 nearby sites, and there was no apparent longitudinal tendency in trends at individual
347 monitoring sites. However, we averaged the observed annual mean surface O₃ at individual
348 monitoring sites at longitudinal intervals (approximately 2.8°) of the model grids as shown by
349 gray rectangles (Fig. 4b) and calculated the long-term trend of averaged monitoring data at
350 each longitudinal band. The calculated increasing trends were clearly larger toward the west,
351 which was consistent with westward rise of the increasing trends of simulated data.

352 There were seasonal differences in the long-term increasing trend of surface O₃ over Japan.
353 The temporal variations of observed and simulated seasonal mean surface O₃ anomalies
354 during 1980–2005 averaged over Japan are shown in Fig. 5. The increasing trend of surface
355 O₃ over Japan in the monitoring data was greatest in spring (March–May: 4.04 ppbv/year) and
356 was also large in summer (June–August: 3.07 ppbv/year); in contrast, increasing trends were
357 relatively small in fall (September–November: 2.29 ppbv/year) and winter (December–
358 February: 1.28 ppbv/year). Seasonal dependency in the increasing trends of observed surface
359 O₃ over Japan has been previously reported (Ohara and Sakata, 2003; ~~Naja and Akimoto,~~
360 ~~2004~~; Parrish et al., 2012). Ohara and Sakata (2003) examined almost the same O₃ monitoring
361 data in Japan as used in the present study for the period 1985–1999 and showed year-round
362 increase in surface O₃ from 1985–1987 to 1997–1999 with a greater increase in the warm
363 season (March–August) than in the rest of the year. ~~Naja and Akimoto (2004) also reported a~~
364 ~~larger increase of O₃ in the warm season between the period 1970–1985 and 1986–2002 in the~~
365 ~~boundary layer over Japan by analyzing ozonesonde data at four sites.~~ Parrish et al. (2012)

366 summarized long-term changes in lower tropospheric baseline O₃ over the world including
367 two regions in Japan (Mt. Happo and several sites in the marine boundary layer grouped as
368 one region), and showed that the increasing trend of surface O₃ was greatest in spring and
369 least in fall in these two regions. In the present study, the simulated increasing trend in
370 seasonal mean surface O₃ was also larger in the warm (spring–summer) than in the cold
371 season (fall–winter), consistent with the observed increasing trends.

372 As described above, our model captured well the basic features of long-term trends in
373 observed surface O₃ over Japan, which allowed us to use the simulated data for further
374 analysis on the source of the long-term trend in the next section.

375

376 **3.2 Contributions of O₃ production regions**

377 The tracer-tagging simulation for 1980–2005 was conducted ~~to examine the long-term~~
378 ~~variations of O₃ tracers tagged by regions of photochemical production, and the~~ IAVs in the
379 annual mean concentrations of each tagged O₃ tracer averaged over Japan are shown in Fig. 6.
380 The tagged tracers other than FT and stratosphere in Fig. 6 and the following figures represent
381 the contribution of O₃ produced in the PBL of different source regions shown in Fig. 1, where
382 contributions of several source regions were grouped into some combined source regions. It
383 should be noted that the model grids used for averaging in these figures differed from those in
384 Figs. 3–5. They encompassed almost all of Japan excluding the Nansei Islands in order to
385 examine temporal behavior of tagged O₃ tracers in all of Japan (see Fig. 4 for actual areas for
386 averaging).

387 Domestically created O₃ was the largest contribution to surface O₃ concentration averaged
388 over Japan during the whole simulation period. The contribution of domestic production had a
389 large IAV and was larger in the last decade (1996–2005) than previously.

390 The second largest contribution was the O₃ created in the FT as a whole during almost the
391 entire period. For the FT, the northern mid-latitude regions such as North Pacific (NPC),
392 Europe (EUR), North Atlantic (NAT), North America (AMN), and China (CHN) made
393 leading contributions during the period; however, the increasing trend of these contributions
394 was considerable particularly for CHN and NPC (Fig. S2). Despite such differences among
395 the regional contributions in the FT, we hereafter only considered the total of each regional
396 contribution in the FT, since it was difficult to associate a regional contribution with a
397 particular source region of O₃ precursor emissions. The precursors eventually resulted in O₃
398 production in a region in the FT can be transported longer distance due to faster wind speed in
399 the FT and therefore would be influenced by emissions from a wider range of source regions
400 than in the PBL. The total FT contribution showed an increasing trend during the period.

401 The NO_x emission from lightning was an indispensable source of NO_x in the FT. The global
402 annual lightning-NO_x emission in the current simulation was about 3.1 TgN/year averaged
403 over the entire period and showed a small but significant increase of about 0.012 TgN/year
404 (0.39 %/year). The increase in lightning-NO_x emission was a consequence of changes in
405 convection activities due to the change in climate forced into the model during the period
406 (~~NCEP/NCAR meteorology and HadISST data~~). However, this increase in lightning-NO_x
407 emission was not the main cause of the increase in the contribution of the total FT – because a
408 sensitivity simulation with all emissions, CH₄ concentration, and stratospheric O₃ fixed at the
409 year 1980 level but with the same temporal evolution in climate showed a quite similar
410 increase in lightning-NO_x emission but no significant increasing trend in the total FT

411 contribution. Therefore, the main cause of the increasing trend in the total FT contribution
412 was likely to be factors other than the increase in lightning-NO_x emission.

413 The contribution of stratospheric O₃ was also large during the entire period, with
414 considerable temporal fluctuations. The large decreases of stratospheric contribution in the
415 early 1980s and 1990s stemmed from the decline of stratospheric O₃ concentration due to the
416 impact of large volcanic eruptions of Mt. El Chichon in 1982 and Mt. Pinatubo in 1991,
417 respectively (Akiyoshi et al., 2009).

418 In the early 1980s, the combined contributions of far remote regions from Japan in the
419 northern mid-latitude (Remote: EUR, NAT, and AMN) made a significant contribution, the
420 fourth largest, to the surface O₃ over Japan and remained at a steady level of contribution
421 during the study period. At the same time, the contribution of CHN significantly increased
422 from the mid-1980s, overtook the contribution of Remote in the early 1990s, and became the
423 largest single regional contribution – excluding the domestic one (i.e., JPN). Moreover, the
424 contributions of O₃ produced in the Korean Peninsula (KOR), the coastal regions in East Asia
425 [E-Asia-Seas: NPC, East China Sea (ECS), and Japan Sea (JPS)], and West-South-SouthEast
426 (WSSE) Asian regions [including Middle East (MES), India (IND), Indochina and Philippines
427 (IDC), and Indonesia etc. (IDN)] also showed obvious increasing trends.

428 The linear trend (ppbv/decade) of annual mean tagged O₃ tracers during the simulation
429 period as well as that of the total O₃, which is the sum of all tagged O₃ tracers averaged over
430 whole Japan (JPN-ALL) and those averaged over three sub-regions in Japan: western (JPN-
431 W), eastern (JPN-E), and northern (JPN-N) Japan is shown in Fig. 7 (see Fig. 4 for the
432 definition of sub-regions). The trend was calculated from the annual mean concentrations.
433 The increasing trend of total O₃ averaged over JPN-ALL was 2.37 ppbv/decade, which was
434 somewhat smaller than estimated in Fig. 3 (2.58 ppbv/decade) due to inclusion of model grids
435 in JPN-N for averaging where the simulated increasing trend of O₃ was relatively small. The
436 increasing trend of total O₃ tended to be greater westward. The absolute contribution of
437 domestically produced O₃ in Japan differed among the regions – it tended to be larger in JPN-
438 E than other parts of Japan (Nagashima et al., 2010); however, there were no such regional
439 differences in long-term trends. The westward tendency of larger increasing trends in total O₃
440 over Japan was mainly due to the similar tendency in the trends of the contribution of CHN,
441 KOR, and E-Asia-Seas, which strongly suggested a large impact of intra-regional
442 transboundary air pollution in East Asia. In particular, the increasing trend in the CHN
443 contribution was the largest for all sub-regions in Japan. The increasing trend in the
444 contributions of total FT and WSSE Asia was slightly smaller for JPN-N than for other parts
445 of Japan, which also contributed to the regional differences of the trend in total O₃ over Japan.
446 ~~Interestingly, the contribution of Remote showed a small but significant increase only in JPN-~~
447 ~~N—although emissions of O₃ precursors, NO_x in particular, in Remote did not increase during~~
448 ~~the period.~~ Due to the large interannual fluctuation, the linear long-term trend of the
449 stratospheric contribution was non-significant for all regions in Japan.

450 The linear trend of tagged O₃ tracers and total O₃ averaged over all of Japan in spring,
451 summer, fall, and winter is shown in Fig. 8. The increasing trends of total O₃ in decreasing
452 order were spring, summer, winter, and fall. This is quite consistent with the seasonal
453 differences in the increasing trend of O₃ observed at several Japanese sites from the 1990s to
454 2011 (Parrish et al., 2012). The increasing trend in the CHN contribution was the largest of all
455 contributions in all four seasons and the trend was particularly large in spring. The KOR
456 contribution was also larger in spring than in other seasons, ~~with the trend in summer of low~~
457 ~~statistical significance due to relatively large IAVs.~~ The contribution of E-Asia-Seas increased

458 significantly in all seasons. Seasonal differences in the increasing trend in the E-Asia-Seas
459 contribution were small, but were slightly larger in the warm (spring–summer) than the cold
460 season (fall–winter). The increasing trend in domestic (JPN) contribution was larger in spring
461 than in summer similarly to the cases of CHN and KOR contributions, but trends in both
462 seasons were non-significant; whereas those in the cold season were significantly larger than
463 in the warm season. The FT and WSSE Asian contributions showed semi-annual change in
464 their increasing trends; larger in summer and winter than in spring and fall. The contribution
465 of Remote showed a significant increasing trend only in winter; ~~conversely that of Central-~~
466 ~~North (CN) Asian regions [Central Asia (CAS) and East Siberia (ESB)] showed small but~~
467 ~~significant decreasing trends in the cold season but non-significant trends in the warm season.~~
468 The seasonal features in each regional contribution described above enabled explanation of
469 the cause of the seasonality of increasing trend in total O₃ over Japan as follows. The largest
470 increasing trend of total O₃ in spring was predominantly attributed to the large increasing
471 trend in contributions of source regions in northeast Asia (CHN, KOR, E-Asia-Seas, and JPN).
472 The increasing trends in the contributions of CHN, KOR, and JPN were smaller in summer,
473 however, partly compensated by the growth of increasing trends in the FT and WSSE Asian
474 contributions from spring to summer. In the cold season, trends for most regions were smaller
475 than in the warm season, except for JPN. The increasing trend in contributions of northeast
476 Asian regions differed little between fall and winter; however, those of FT, WSSE Asia, and
477 Remote had larger increasing trends in winter than in fall, which made the increasing trend of
478 total O₃ in winter larger than in fall.

479 Table 1 summarizes the linear trends of annual mean tagged O₃ tracers and the total O₃
480 averaged over JPN-ALL. The vast majority (about 97 %) of the trend in total O₃ was balanced
481 with the sum of those trends in regional contributions with statistical significance. The largest
482 contribution was from the increase of O₃ produced in CHN (0.85 ppbv/decade), which
483 corresponded to about 36 % of the increasing trend of total O₃. The increasing trend in the
484 contribution of the total FT was also large (0.37 ppbv/decade), representing about 16 % of the
485 total O₃ trend. The contributions of northeast Asian regions other than CHN also increased
486 significantly (0.34, 0.29, and 0.27 ppbv/decade for KOR, E-Asia-Seas, and JPN, respectively)
487 and each accounted for about 12–15 % of the total O₃ trend. About 7 % of the total O₃ trend
488 was attributable to the increasing trend in WSSE Asian contributions (0.16 ppbv/decade). The
489 linear trends in the contributions of remaining regions [~~CN-Asia, Remote, stratosphere, and~~
490 ~~the others (OTH)] were small and non-significant, and so were not important concerning the
491 cause of reported surface O₃ increase over Japan.~~

492

493 **3.3 Impact of ~~IAVs-temporal variations~~ in O₃ precursor emissions in different** 494 **source regions on regional O₃ production**

495 The results in the preceding section revealed the relative importance of O₃ produced in
496 different regions to the recent increasing trend in surface O₃ over Japan. It is noteworthy that
497 this does not indicate the relative importance of the different regions of O₃ precursor
498 emissions. For example, there were significant contributions of E-Asia-Seas to the increasing
499 trend in surface O₃ over Japan, but there were clearly no large emission sources of precursors
500 in these maritime regions other than navigation. The increasing trend in the contribution of E-
501 Asia-Seas was likely a consequence of increased transport of O₃ precursors to this region,
502 which had been emitted in adjacent land areas. However, the tracer-tagging approach cannot
503 distinguish the differences in origins of emissions of precursors that resulted in O₃ production
504 in E-Asia-Seas. To further investigate the roles of different regions in the recent increasing

505 trend of surface O₃ over Japan, we performed a series of sensitivity simulations with different
506 assumptions for the temporal variation of factors, which would affect the surface O₃ over
507 Japan. Each sensitivity simulation consisted of a 26-year simulation with full-chemistry setup
508 of CHASER followed by another 26-year simulation with tracer-tagging setup of CHASER.
509 Initially, a sensitivity simulation was performed that was only forced by the IAVs in the
510 climate (~~NCEP/NCAR meteorology and HadISST data~~) but with all emissions of O₃
511 precursors, CH₄ concentration, and stratospheric O₃ fixed at the year 1980 level; then we
512 gradually added the ~~increase of the IAV~~temporal variation of chemical factors as summarized
513 in Table 2. The simulation F, driven by the ~~IAV~~temporal variation of all forcings, was
514 identical to the standard simulation; and simulation A was mentioned concerning lightning-
515 NO_x emission in the preceding section (3.2).

516 The linear trends of annual mean total O₃ and tagged O₃ tracers that had significant effects
517 on the standard simulation averaged over all of Japan in all simulations are shown and
518 compared in Fig. 9. Simulation A showed no obvious increasing trend in total O₃ over Japan.
519 The surface temperature over Japan in the model which was assimilated into NCEP/NCAR
520 reanalysis data showed a warming of 0.44 ± 0.21 °C/decade in the annual mean during the
521 simulation period which well corresponded to the observed warming of 0.45 ± 0.23 °C/decade
522 (JMA, 2017). The IAV of the surface temperature was well captured by the model too,
523 although the modelled temperature was somewhat warmer than the observation in 2000s
524 particularly in winter which might be related to the slight overestimation of winter surface O₃
525 in the model depicted in Fig.5. The JPN and total FT contributions exhibited increasing trends
526 (0.12 and 0.06 ppbv/decade, respectively), likely due to the IAV of the climate, but they were
527 non-significant.

528 The increase in atmospheric concentration of CH₄ was added in simulation B, because this
529 would have a non-negligible impact on tropospheric O₃ (background O₃ in particular), as
530 frequently reported (Brasseur et al., 2006; Kawase et al., 2011; HTAP, 2010 and references
531 therein). In the simulations other than A, we used a CH₄ concentration increase rate of about
532 12.3 ppbv/year (0.73 %/year) during 1980–2000 and flattened thereafter. In simulation B, the
533 contribution of the total FT showed a significant increasing trend (0.18 ppbv/decade) as did
534 that of Remote (0.08 ppbv/decade; data not shown). The contributions of several other regions
535 such as CHN, E-Asia-Seas, and WSSE Asia also showed slight increasing trends
536 (approximately 0.01–0.02 ppbv/decade), although non-significant. Note that these values
537 included the impact of CH₄ increase as well as the IAV of the climate and, consequently, the
538 total O₃ in simulation B showed a significant increasing trend of about 0.44 ppbv/decade,
539 representing about 19 % of the increasing trend in total O₃ in the standard simulation (2.37
540 ppbv/decade).

541 In simulations C–E, the ~~IAVs~~temporal variations in emission of O₃ precursors in northeast
542 Asian regions were gradually added: CHN, KOR, and JPN, respectively. The increase in
543 emissions of O₃ precursors in CHN in simulation C caused a large significant increasing trend
544 in the contribution of CHN itself (0.83 ppbv/decade). Moreover, the emission increase in
545 CHN also had a large impact on the contributions of other regions, in particular, the increase
546 trends in the contributions of KOR and E-Asia-Seas became significant: 0.12 and 0.15
547 ppbv/decade, respectively. The JPN and the total FT contributions also showed somewhat
548 larger increasing trends in simulation C than in B, but the growth in trends between the two
549 simulations was not as large as those of KOR and E-Asia-Seas. The total effect of the
550 emission increase in CHN on the increasing trend in surface O₃ over Japan, assessed using the
551 difference in total O₃ trend between simulations B and C, was about 1.08 ppbv/decade and
552 corresponded to about 46 % of the increasing trend in total O₃ in the standard simulation. The

553 relative contribution of CHN as a source region of O₃ production to the surface O₃ increasing
554 trend over Japan was estimated as 36 % in the preceding section (3.2); however, the
555 contribution of CHN as a source region of O₃ precursors emission was somewhat (10 %)
556 larger due to the production of O₃ outside CHN. It is noteworthy that the slight increasing
557 trend in the contribution of WSSE Asia shown in the CH₄ increase in simulation B was
558 smaller in simulation C. The contributions of Remote and the stratosphere showed similar
559 responses. The increase in O₃ precursor emissions in CHN seemed to partly offset the
560 increase in influence of long range transport of O₃ from such regions.

561 The increase in emissions from KOR in addition to CHN in simulation D gave rise to a
562 much larger increasing trend in the contributions of KOR itself (0.38 ppbv/decade).
563 Compared with simulation C (0.12 ppbv/decade), about one-third of the increasing trend in
564 the contribution of KOR was attributed to the O₃ precursor emission increase in CHN and the
565 rest to emission increase in KOR. Similarly, the emission increase in KOR caused a larger
566 increasing trend in the contributions of E-Asia-Seas in simulation D (0.25 ppbv/decade). We
567 attributed about half of the increasing trend in the contribution of E-Asia-Seas in the standard
568 simulation (0.29 ppbv/decade) to the impact of O₃ precursor emission increase in CHN (and
569 partly that of the CH₄ increase: 0.15 ppbv/decade) as shown in simulation C, about one-third
570 to that in KOR, and the rest to that in regions other than northeast Asia. By further adding the
571 IAV-temporal variation in the domestic (JPN) emissions in simulation E, the increasing trend
572 in the domestic contribution became significant (0.28 ppbv/decade), implying that the
573 increasing trend in domestically produced O₃ was from a combination of multiple factors each
574 of which did not cause a significant increase. The total effect of the emission increase in KOR
575 on the increasing trend in surface O₃ over Japan assessed as the difference between
576 simulations C and D was about 0.38 ppbv/decade; and that of the IAV of domestic emission
577 in Japan assessed as the difference between simulations D and E was about 0.09 ppbv/decade;
578 each of which corresponded to about 16 and 4 % of the increasing trend in total O₃ in the
579 standard simulation, respectively.

580 The IAV in emissions of O₃ precursors in northeast Asian regions (CHN, KOR, and JPN)
581 together with the IAV in the climate and the increase in CH₄ concentration induced a
582 significant increasing trend in total O₃ over Japan with a rate of 1.99 ppbv/decade. This
583 accounted for about 84 % of the increasing trend in total O₃ in the standard simulation. The
584 rest of the increasing trend should be regarded as from O₃ precursor emission changes in
585 regions other than northeast Asia. The difference between simulations E and F (standard
586 simulation) showed that the emission change in such regions influenced surface O₃ over Japan
587 mainly through increasing the O₃ production in WSSE Asia and the FT (Fig. 9).

588

589 **4 Summary and conclusion**

590 We demonstrated the relative importance of the regions of photochemical O₃ production in
591 the global atmosphere on the long-term increasing trend in surface O₃ over Japan reported in
592 recent decades by conducting a series of tracer-tagging simulations using the global CTM
593 CHASER. The impact of the IAVs of climate, of CH₄ concentration, and of emission of O₃
594 precursors (NO_x and NMVOC) in different source regions on regional photochemical O₃
595 production were also investigated.

596 The observed increasing trend of surface O₃ over Japan for 1980–2005 (2.70 ppbv/decade
597 for annual mean over whole Japan) was successfully reproduced by the model (2.58
598 ppbv/decade) including an obvious tendency of increase toward western Japan and to be
599 greater in the warm (spring–summer) than in the cold season (fall–winter).

600 The absolute contribution of each photochemical O₃ production region to the surface O₃ over
601 Japan represented by the concentrations of tagged O₃ tracer showed different temporal
602 evolution by regions. The contributions of all Asian regions except the northern part (i.e.,
603 CHN, KOR, E-Asia-Seas, JPN, and WSSE) as well as those of the total FT exhibited
604 significant increasing trends during the period. The increasing trend in the contribution of
605 domestically produced O₃ in Japan (i.e., JPN) did not differ much among the different regions
606 in Japan. However, there was a tendency in the increasing trends in contributions of CHN,
607 KOR, and E-Asia-Seas to be large toward western Japan, which was a main cause of the same
608 tendency in the increasing trend in total O₃ and suggested a large impact of intra-regional
609 transboundary air pollution in East Asia.

610 The trends in contributions of most O₃ production regions, except JPN, were larger in the
611 warm than in the cold season, providing a basis for the seasonality in the increasing trend in
612 total O₃ over Japan. Thus, the larger increasing trend of total O₃ in spring than in summer was
613 mainly due to the same tendency in increasing trends in the contributions of northeast Asian
614 regions (CHN, KOR, and JPN), although this was partly compensated by larger increasing
615 trends in the FT and WSSE Asia contributions in summer than spring. In the cold season, the
616 contributions of FT, WSSE Asia, and Remote had larger increasing trends in winter than in
617 fall, which led to a larger increasing trend in total O₃ in winter than in fall.

618 The sum of the trends in contributions of O₃ production regions with sufficient statistical
619 significance accounted for most (about 97 %) of the increasing trend in total O₃ over Japan
620 (2.37 ppbv/decade). The largest portion was attributed to the increasing trend of O₃ produced
621 in CHN (36 %; 0.85 ppbv/decade), followed by that in the total FT (16 %; 0.37 ppbv/decade).
622 The increasing trend in contributions of the other northeast Asian regions (KOR, E-Asia-Seas,
623 and JPN; 0.27–0.34 ppbv/decade) each accounted for about 12–15 % of the total O₃ trend, and
624 the majority of the rest of the total O₃ trend (7 %; 0.16 ppbv/decade) was attributable to
625 WSSE Asia.

626 We further investigated the impact of the IAV-temporal variation of controlling factors, such
627 as climate, CH₄ concentration, and emission of O₃ precursors, on photochemical O₃
628 production in different source regions and its influence on the long-term increasing trend in
629 surface O₃ over Japan through a series of sensitivity simulations that gradually added the IAV
630 temporal variation of these factors. The IAV of the climate and the increase in CH₄
631 concentration together caused the increase of photochemical O₃ production in several regions
632 and resulted in the significant increasing trend in surface O₃ over Japan (0.44 ppbv/decade)
633 and represented about 19 % of the increasing trend in surface O₃ in the standard simulation.
634 The increase in emission of O₃ precursors in CHN led to the increase of photochemical O₃
635 production in northeast Asian regions including CHN itself, KOR, JPN, and E-Asia-Seas; and
636 the resulting increasing trend in surface O₃ over Japan (1.08 ppbv/decade) accounted for
637 about 46 % of that in the standard simulation. The relative contribution of CHN to the surface
638 O₃ increasing trend over Japan as the source region of O₃ precursor “emission” was 10 %
639 larger than as the source region of O₃ “production” due to production of O₃ outside of CHN.
640 Then, the impact of the O₃ precursor emission change in KOR and JPN on the increasing
641 trend in surface O₃ over Japan (about 0.38 and 0.10 ppbv/decade, respectively) corresponded
642 to 16 and 4 % of the increasing trend in total O₃ in the standard simulation, respectively. The
643 rest of the increasing trend in total O₃ in the standard simulation (about 16 %) was attributed
644 to O₃ precursor emission change in regions other than northeast Asia, mainly through
645 increasing the photochemical O₃ production in WSSE Asia and the total FT.

646 The results summarized above depended largely on the forcings of long-term simulation,
647 particularly the long-term variation of the emissions of O₃ precursors in Asia. Zhao et al.
648 (2013) estimated the NO_x emission in China for the period 1995–2010 and compared it to the
649 existing emission inventories including Hao et al. (2002), Zhan et al. (2007), and the version
650 of REAS used in this study. They showed the long-term increasing trend in Chinese NO_x
651 emission in REAS was consistent with that in the other inventories, but the amount of
652 emission was somewhat smaller in REAS than in the others. Therefore, the long-term
653 increasing trend in the contribution of Chinese emission to the surface O₃ over Japan showed
654 in the preset study would be retained if the other emission inventories were used for the
655 simulation but the specific values of the contributions could be affected. Further studies
656 should address the impact these uncertainties in the different emission inventories on the trend
657 of surface O₃ over Japan.

658

659 *Acknowledgements.* This research was supported by the Global Environment Research Fund
660 (S-7) by the Ministry of the Environment (MOE) of Japan and the East Asian Environment
661 Research Program at the National Institute for Environmental Studies (NIES). We
662 acknowledge the entire staff of the EANET and the AEROS air quality monitoring stations of
663 the MOE of Japan and of the local governments for carrying out measurements and providing
664 the observations. The calculations were performed on the NIES supercomputer system (NEC
665 SX-8R, SX9). The GFD-DENNOU library was used for drawing the figures.

666

667 **References**

- 668 Akimoto, H., Mori, Y., Sasaki, K., Nakanishi, H., Ohizumi, T., and Itano, Y.: Analysis of
669 monitoring data of ground-level ozone in Japan for longterm trend during 1990–2010:
670 Causes of temporal and spatial variation, *Atmos. Environ.*, 102, 302–310, 2015.
- 671 Akiyoshi, H., Zhou, L. B., Yamashita, Y., Sakamoto, K., Yoshiki, M., Nagashima, T.,
672 Takahashi, T., Kurokawa, J., Takigawa, M., and T. Imamura, T.: A CCM simulation of the
673 breakup of the Antarctic polar vortex in the years 1980–2004 under the CCMVal scenarios,
674 *J. Geophys. Res.*, 114, D03103, doi:10.1029/2007JD009261, 2009.
- 675 Brasseur, G. P., Schultz, M., Granier, C., Saunois, M., Diehl, T., Botzet, M., and Roeckner,
676 E.: Impact of climate change on the future chemical composition of the global troposphere,
677 *J. Clim.*, 19, 3932–3951, doi:10.1175/JCLI3832.1, 2006.
- 678 Chang, S.-C. and Lee, C.-T.: Evaluation of the trend of air quality in Taipei, Taiwan from
679 1994 to 2003, *Environ. Monit. Assess.*, 127, 87–96, doi:10.1007/s10661-006-9262-1, 2007.
- 680 Chou, C. C.-K., Liu, S. C., Lin, C.-Y., Shiu, C.-J., and Chang, K.-H.: The trend of surface
681 ozone in Taipei, Taiwan, and its causes: Implications for ozone control strategies, *Atmos.*
682 *Environ.*, 40, 3898–3908, 2006.
- 683 Cooper, O. R., Parrish, D. D., Ziemke, J., Balashov, N. V., Cupeiro, M., Galbally, I. E., Gilge,
684 S., Horowitz, L., Jensen, N. R., Lamarque, J.-F., Naik, V., Oltmans, S. J., Schwab, J.,
685 Shindell, D. T., Thompson, A. M., Thouret, V., Wang, Y., and Zbinden, R. M.: Global
686 distribution and trends of tropospheric ozone: An observation-based review, *Elementa*, 2,
687 000029, doi: 10.12952/journal.elementa.000029, 2014.
- 688 Ding, A. J., Wang, T., Thouret, V., Cammas, J.-P., and Nédélec, P.: Tropospheric ozone
689 climatology over Beijing: analysis of aircraft data from the MOZAIC program, *Atmos.*
690 *Chem. Phys.*, 8, 1–13, 2008.
- 691 Eyring, V., Harris, N. R. P., Rex, M., Shepherd, T. G., Fahey, D. W., Amanatidis, G. T.,
692 Austin, J., Chipperfield, M. P., Dameris, M., Forster, P. M. De F., Gettelman, A., Graf, H.
693 F., Nagashima, T., Newman, P. A., Pawson, S., Prather, M. J., Pyle, J. A., Salawitch, R. J.,
694 Santer, B. D., and Waugh, D. W.: A strategy for process-oriented validation of coupled
695 chemistry-climate models. *Bull. Am. Meteorol. Soc.*, 86, 1117–1133, 2005.

696 [Hao, J. M., Tian, H. Z., and Lu, Y. Q.: Emission inventories of NO_x from commercial energy](#)
697 [consumption in China, 1995–1998, *Environ. Sci. Technol.*, 36, 552–560,](#)
698 [doi:10.1021/Es015601k, 2002.](#)

699 HTAP, UNECE: Hemispheric Transport of Air Pollution 2010: Part A: Ozone and Particulate
700 Matter, Air Pollution Studies No. 17, (ed. by Dentener, F., Keating, T., and Akimoto, H.),
701 ECE/EN.Air/100, 2010.

702 [JMA \(Japan Meteorological Agency\): available online at](#)
703 http://www.data.jma.go.jp/cpdinfo/temp/list/an_jpn.html (In Japanese), 2017.

704 Kalnay, E., Kanamitsu, M., Kistler, R., Collins, W., Deaven, D., Gandin, L., Iredell, M., Saha,
705 S., White, G., Woollen, J., Zhu, Y., Leetmaa, A., Reynolds, B., Chelliah, M., Ebisuzaki,
706 W., Higgins, W., Janowiak, J., Mo, K. C., Ropelewski, C., Wang, J., Jenne, R., and Joseph,
707 D.: The NCEP/NCAR 40-year reanalysis project, *Bull. Amer. Meteor. Soc.*, 77, 437–470,
708 1996.

709 Kawase, H., Nagashima, T., Sudo, K., and Nozawa, T.: Future changes in tropospheric ozone
710 under Representative Concentration Pathways (RCPs), *Geophys. Res. Lett.*, 38, L05801,
711 doi:10.1029/2010GL046402, 2011.

712 Kurokawa, J., Ohara, T., Uno, I., Hayasaka, M., and Tanimoto, H.: Influence of
713 meteorological variability on interannual variations of springtime boundary layer ozone
714 over Japan during 1981–2005, *Atmos. Chem. Phys.*, 9, 6287–6304, 2009.

715 Kurokawa, J., Ohara, T., Morikawa, T., Hanayama, S., Janssens-Maenhout, G., Fukui, T.,
716 Kawashima, K., and Akimoto, H.: Emissions of air pollutants and greenhouse gases over
717 Asian regions during 2000–2008: Regional Emission inventory in ASia (REAS) version 2,
718 *Atmos. Chem. Phys.*, 13, 11019–11058, 2013.

719 Lee, H.-J., Kim, S.-W., Brioude, J., Cooper, O. R., Frost, G. J., Kim, C.-H., Park, R. J.,
720 Trainer, M., and Woo J.-H.: Transport of NO_x in East Asia identified by satellite and in
721 situ measurements and Lagrangian particle dispersion model simulations, *J. Geophys. Res.*
722 *Atmos.*, 119, 2574–2596, doi:10.1002/2013JD021185, 2014.

723 Li, J., Wang, Z. F., Akimoto, H., Yamaji, K., Takigawa, M., Pochanart, P., Liu, Y., Tanimoto,
724 H., and Kanaya, Y.: Near-ground ozone source attributions and outflow in central eastern
725 China during MTX2006, *Atmos. Chem. Phys.*, 8, 7335–7351, 2008.

726 Li, H. C., Chen, K. S., Huang, C. H., and Wang, H. K.: Meteorologically adjusted long-term
727 trend of ground-level ozone concentrations in Kaohsiung County, southern Taiwan, *Atmos.*
728 *Environ.*, 44, 3605–3608, 2010.

729 Lin, S.-J. and Rood, R. B.: Multidimensional flux-form semi-Lagrangian transport scheme,
730 *Mon. Weather Rev.*, 124, 2046–2070, 1996.

731 Lin, Y.-K., Lin, T.-H., and Chang, S.-C.: The changes in different ozone metrics and their
732 implications following precursor reductions over northern Taiwan from 1994 to 2007,
733 *Environ. Monit. Assess.*, 169, 143–157, 2010.

734 Logan, J. A., Megretskaia, I. A., Miller, A. J., Tiao, G. C., Choi, D., Zhang, L., Stolarski, R.
735 S., Labow, G. J., Hollandsworth, S. M., Bodeker, G. E., Claude, H., de Muer, D., Kerr, J.
736 B., Tarasick, D. W., Oltmans, S. J., Johnson, B., Schmidlin, F., Staehelin, J., Viatte, P., and
737 Uchino, O.: Trends in the vertical distribution of ozone: A comparison of two analyses of
738 ozonesonde data, *J. Geophys. Res.*, 104, 26373–26399, 1999.

739 Lu, W.-Z. and Wang, X.-K.: Evolving trend and self-similarity of ozone pollution in central
740 Hong Kong ambient during 1984–2002, *Sci. Total Environ.*, 357, 160–168, 2006.

741 Mauzerall, D. L., Sultan, B., Kim, N., and Bradford, D. F.: NO_x emissions from large point
742 sources: variability in ozone production, resulting health damages and economic costs,
743 *Atmos. Environ.*, 39, 2851–2866, 2005.

744 Meinshausen, M., Smith, S. J., Calvin, K., Daniel, J. S., Kainuma, M. L. T., Lamarque, J.-F.,
745 Matsumoto, K., Montzka, S. A., Raper, S. C. B., Riahi, K., Thomson, A., Velders, G. J. M.,
746 and van Vuuren, D. P. P.: The RCP greenhouse gas concentrations and their extensions
747 from 1765 to 2300, *Climatic Change*, 109, 213–241, 2011.

748 MOE (Ministry of Environment) Japan: FY 2013 status of air pollution, available online at:
749 <http://www.env.go.jp/air/osen/jokyoh25/> (in Japanese), 2013.

750 Nagashima, T., Ohara, T., Sudo, K., and Akimoto, H.: The relative importance of various
751 source regions on East Asian surface ozone, *Atmos. Chem. Phys.*, 10, 11305–11322, 2010.

752 Naja, M. and Akimoto, H.: Contribution of regional pollution and long-range transport to the
753 Asia-Pacific region: Analysis of long-term ozonesonde data over Japan, *J. Geophys. Res.*,
754 109, D21306, doi:10.1029/2004JD004687, 2004.

755 Nozawa, T., Nagashima, T., Shiogama, H., and Crooks, S. A.: Detecting natural influence on
756 surface air temperature change in the early twentieth century, *Geophys. Res. Lett.*, 32,
757 L20719, doi:10.1029/2005GL023540, 2005.

758 Ohara, T. and Sakata, T.: Long-term variation of photochemical oxidants over Japan, *J. Jpn.*
759 *Soc. Atmos. Environ.*, 38, 47–54. (in Japanese with English summary), 2003.

760 Ohara, T., Yamaji, K., Uno, I., Tanimoto, H., Sugata, S., Nagashima, T., Kurokawa, J., Horii,
761 N., and Akimoto, H.: Long-term simulations of surface ozone in East Asia during 1980–
762 2020 with CMAQ and REAS inventory, In *Air Pollution Modelling and Its Application*
763 *XIX (NATO Science for Peace and Security Series C: Environmental Security)* (ed. by
764 Borrego, C., and Miranda, A. I.). Springer, Dordrecht, The Netherlands, 136–144, 2008.

765 Ohara, T., Akimoto, H., Kurokawa, J., Horii, N., Yamaji, K., Yan, X., and Hayasaka, T.: An
766 Asian emission inventory of anthropogenic emission sources for the period 1980–2002,
767 *Atmos. Chem. Phys.*, 7, 4410–4444, 2007.

768 Olivier, J. G. J. and Berdowski, J. J. M.: Global emissions sources and sinks, in: *The Climate*
769 *System*, Berdowski, J., Guicherit, R., and Heij, B. J. (eds.), A. A. Balkema Publishers/
770 Swets & Zeitlinger Publishers, Lisse, The Netherlands, 33–78, 2001.

771 Oltmans, S. J., Lefohn, A. S., Harris, J. M., Galbally, I., Scheel, H. E., Bodeker, G., Brunke,
772 E., Claude, H., Tarasick, D., Johnson, B. J., Simmonds, P., Shadwick, D., Anlauf, K.,
773 Hayden, K., Schmidlin, F., Fujimoto, T., Akagi, K., Meyer, C., Nichol, S., Davies, J.,
774 Redondas, A., and Cuevas, E.: Long-term changes in tropospheric ozone, *Atmos. Environ.*,
775 40, 3156–3173, 2006.

776 Oltmans, S. J., Lefohn, A. S., Shadwick, D., Harris, J. M., Scheel, H. E., Galbally, I., Tarasick,
777 D. W., Johnson, B. J., Brunke, E.-G., Claude, H., Zeng, G., Nichol, S., Schmidlin, F.,
778 Davies, J., Cuevas, E., Redondas, A., Naoe, H., Nakano, T., and Kawasato, T.: Recent
779 tropospheric ozone changes – A pattern dominated by slow or no growth, *Atmos. Environ.*,
780 67, 331–351, 2013.

781 Parrish, D. D., Law, K. S., Staehelin, J., Derwent, R., Cooper, O. R., Tanimoto, H., Volz-
782 Thomas, A., Gilge, S., Scheel, H.-E., Steinbacher, M., and Chan, E.: Long-term changes in
783 lower tropospheric baseline ozone concentrations at northern mid-latitudes, *Atmos. Chem.*
784 *Phys.*, 12, 11485–11504, 2012.

785 Rayner, N. A., Parker, D. E., Horton, E. B., Folland, C. K., Alexander, L. V., Rowell, D. P.,
786 Kent, E. C., and Kaplan, A.: Global analyses of sea surface temperature, sea ice, and night
787 marine air temperature since the late nineteenth century, *J. Geophys. Res.*, 108, 4407,
788 doi:10.1029/2002JD002670, 2003.

789 Schultz, M. G., Heil, A., Hoelzemann, J. J., Spessa, A., Thonicke, K., Goldammer, J. G., Held,
790 A. C., Pereira, J. M. C., and van het Bolscher, M.: Global wildland fire emissions from
791 1960 to 2000, *Global Biogeochem. Cycles*, 22, GB2002, doi:10.1029/2007GB003031,
792 2008.

793 Seo, J., Youn, D., Kim, J. Y., and Lee, H.: Extensive spatiotemporal analyses of surface
794 ozone and related meteorological variables in South Korea for the period 1999–2010,
795 *Atmos. Chem. Phys.*, 14, 6395–6415, 2014.

796 Shindell, D., Kuylenstierna, J. C. I., Faluvegi, G., Milly, G., Emberson, L., Hicks, K., Vignati,
797 E., Van Dingenen, R., Janssens-Maenhout, G., Raes, F., Pozzoli, L., Amann, M., Klimont,
798 Z., Kupiainen, K., Höglund-Isaksson, L., Anenberg, S. C., Muller, N., Schwartz, J., Streets,
799 D., Ramanathan, V., Oanh, N. T. K., Williams, M., Demkine, V., and Fowler, D.:
800 Simultaneously mitigating near-term climate change and improving human health and food
801 security, *Science*, 335, 183–189, 2012.

802 Silva, R. A., West, J. J., Zhang, Y., Anenberg, S. C., Lamarque, J.-F., Shindell, D. T., Collins,
803 W. J., Dalsoren, S., Faluvegi, G., Folberth, G., Horowitz, L. W., Nagashima, T., Naik, V.,
804 Rumbold, S., Skeie, F., Sudo, K., Takemura, T., Bergmann, D., Cameron-Smith, P., Cionni,
805 I., Doherty, R. M., Eyring, V., Josse, B., MacKenzie, I. A., Plummer, D., Righi, M.,
806 Stevenson, D. S., Strode S., Szopa, S., and Zeng, G.: Global premature mortality due to
807 anthropogenic outdoor air pollution and the contribution of past climate change, *Environ.*
808 *Res. Lett.*, 8, 034005, 2013.

809 Sudo, K. and Akimoto, H.: Global source attribution of tropospheric ozone: Long-range
810 transport from various source regions, *J. Geophys. Res.*, 112, D12302,
811 doi:10.1029/2006JD007992, 2007.

812 Sudo, K., Takahashi, M., Kurokawa, J., and Akimoto, H.: CHASER: A global chemical
813 model of the troposphere: 1. Model description, *J. Geophys. Res.*, 107(D17), 4339,
814 doi:10.1029/2001JD001113, 2002.

815 Susaya, J., Kim, K.-H., Shon, Z.-H., and Brown, R. J. C.: Demonstration of long-term
816 increases in tropospheric O₃ levels: Causes and potential impacts, *Chemosphere*, 92, 1520–
817 1528, 2013.

818 Tanimoto, H.: Increase in springtime tropospheric ozone at a mountainous site in Japan for
819 the period 1998–2006, *Atmos. Environ.*, 43, 1358–1363, 2009.

820 Tanimoto, H., Ohara, T., and Uno, I.: Asian anthropogenic emissions and decadal trends in
821 springtime tropospheric ozone over Japan: 1998–2007, *Geophys. Res. Lett.*, 36, L23802,
822 doi:10.1029/2009GL041382, 2009.

823 UNEP (United Nations Environment Programme) and WMO (World Meteorological
824 Organization): Integrated Assessment of Black Carbon and Tropospheric Ozone: Summary
825 for Decision Makers, available online at
826 http://www.unep.org/dewa/Portals/67/pdf/Black_Carbon.pdf, 2011.

827 US EPA (U.S. Environmental Protection Agency): Air Quality Criteria for Ozone and Related
828 Photochemical Oxidants (Final), U.S. Environmental Protection Agency, Washington, DC,
829 EPA/600/R-05/004aF-cF, 2006.

830 Van Aardenne, J. A., Dentener, F. J., Olivier, J. G. J., Klein Goldewijk, C. G. M., and
831 Lelieveld, J.: A 1 x 1 degree resolution dataset of historical anthropogenic trace gas
832 emissions for the period 1890–1990, *Global Biogeochem. Cy.*, 15(4), 909–928, 2001.

833 Van Leer, B.: Toward the ultimate conservative difference scheme. IV: A new approach to
834 numerical convection, *J. Comput. Phys.*, 23, 276–299, 1977.

835 Wakamatsu, S., Morikawa, T., and Ito, A.: Air Pollution Trends in Japan between 1970 and
836 2012 and Impact of Urban Air Pollution Countermeasures, *Asian J. Atmos. Env.*, 7(4),
837 177–190, 2013.

838 Wang, X. and Mauzerall, D. L.: Characterizing distributions of surface ozone and its impact
839 on grain production in China, Japan and South Korea: 1990 and 2020, *Atmos. Environ.*, 38,
840 4383–4402, 2004.

841 Wang, T., Wei, X. L., Ding, A. J., Poon, C. N., Lam, K. S., Li, Y. S., Chan, L. Y., and Anson,
842 M.: Increasing surface ozone concentrations in the background atmosphere of Southern
843 China, 1994–2007, *Atmos. Chem. Phys.*, 9, 6217–6227, 2009.

844 Wang, Y., Zhang, Y., Hao, J., and Luo, M.: Seasonal and spatial variability of surface ozone
845 over China: contributions from background and domestic pollution, *Atmos. Chem. Phys.*,
846 11, 3511–3525, 2011.

847 Xu, X., Lin, W., Wang, T., Yan, P., Tang, J., Meng, Z., and Wang, Y.: Long-term trend of
848 surface ozone at a regional background station in eastern China 1991–2006: enhanced
849 variability, *Atmos. Chem. Phys.*, 8, 2595–2607, 2008.

850 [Zhang, Q., Streets, D. G., He, K., Wang, Y., Richter, A., Burrows, J. P., Uno, I., Jang, C. J.,](#)
851 [Chen, D., Yao, Z., and Lei, Y.: NO_x emission trends for China, 1995–2004: The view from](#)
852 [the ground and the view from space, *J. Geophys. Res.-Atmos.*, 112,](#)
853 [doi:10.1029/2007jd008684, 2007.](#)

854 Zhang, Q., Yuan, B., Shao, M., Wang, X., Lu, S., Lu, K., Wang, M., Chen, L., Chang, C.-C.,
855 and Liu, S. C.: Variations of ground-level O₃ and its precursors in Beijing in summertime
856 between 2005 and 2011, *Atmos. Chem. Phys.*, 14, 6089–6101, 2014.

857 [Zhao, B., Wang, S. X., Liu, H., Xu, J. Y., Fu, K., Klimont, Z., Hao, J. M., He, K. B., Cofala,](#)
858 [J., and Amann M.: NO_x emissions in China: historical trends and future perspectives,](#)
859 [*Atmos. Chem. Phys.*, 13, 9869–9897, 2013.](#)

860

861

862 **Table 1.** Summary of the linear trends of annual mean tagged O₃ tracers as well as the total O₃
 863 averaged over Japan (JPN-ALL) for 1980–2005. Bold figures denote that trends are
 864 significant at 5 % risk level.

Source Region	Trend [ppbv/dec]	Percent
CHN	0.85 ± 0.2	35.8
KOR	0.34 ± 0.14	14.6
JPN	0.27 ± 0.19	11.5
E-Asia-Seas	0.29 ± 0.05	12.4
WSSE Asia	0.16 ± 0.04	6.8
CN Asia	-0.05 ± 0.08	-2.1
Remote	0.04 ± 0.08	1.7
OTH	0.01 ± 0.02	0.5
FT	0.37 ± 0.1	15.5
Strat.	0.08 ± 0.28	3.3
Total	2.37 ± 0.42	100.0

865

866

867 **Table 2.** Summary of the sensitivity simulations and the standard simulation

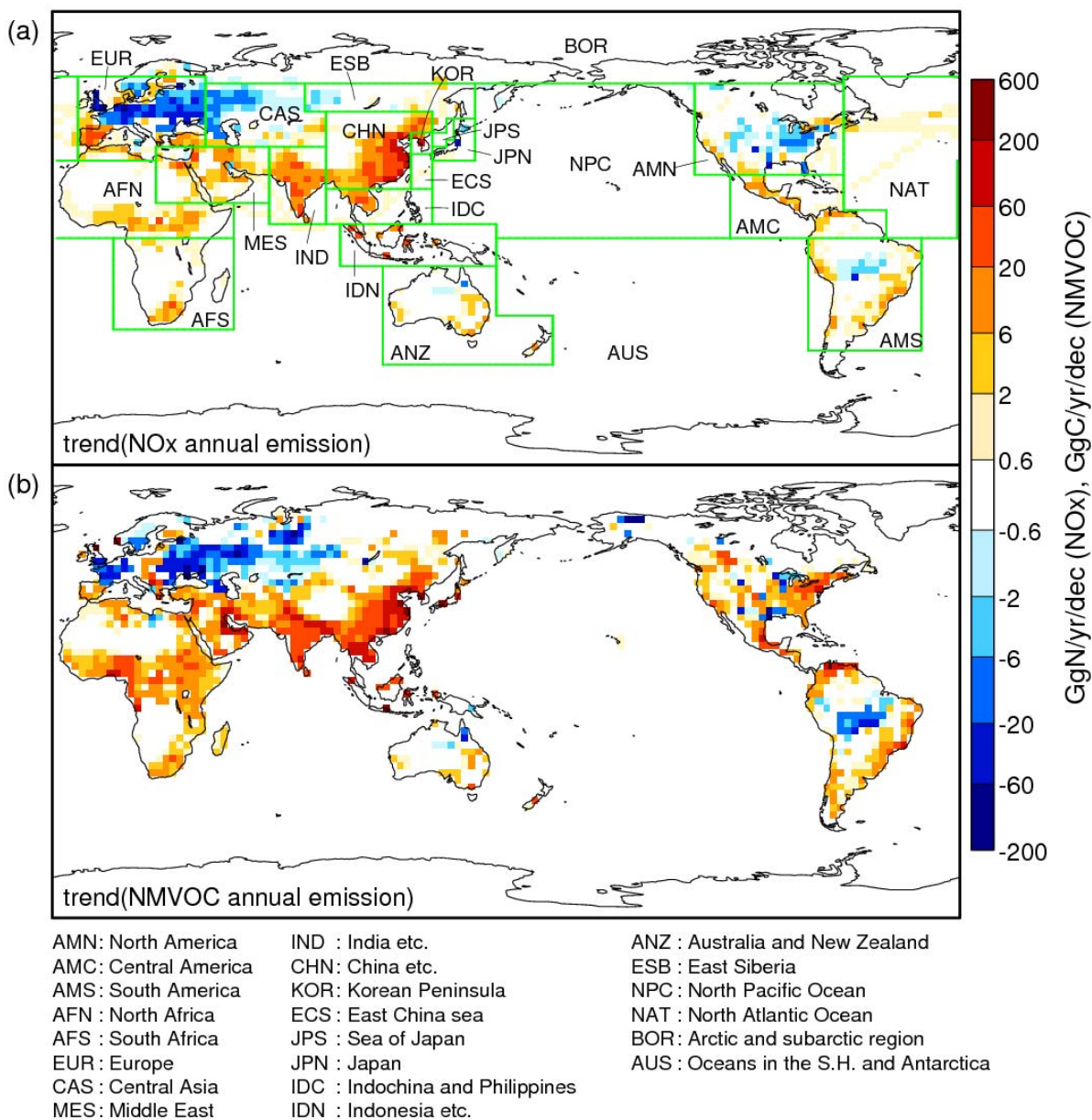
Simulation code	CH ₄ concentration	O ₃ precursor emissions				Stratospheric O ₃ trend
		CHN	KOR	JPN	ROW ^a	
A	1980 ^b	1980	1980	1980	1980	1980
B	increase ^c	1980	1980	1980	1980	1980
C	increase	IAV ^d <u>Var</u> ^d	1980	1980	1980	1980
D	increase	IAV <u>Var</u>	IAV <u>Var</u>	1980	1980	1980
E	increase	IAV <u>Var</u>	IAV <u>Var</u>	IAV <u>Var</u>	1980	1980
F (standard)	increase	IAV <u>Var</u>	IAV <u>Var</u>	IAV <u>Var</u>	IAV <u>Var</u>	IAV <u>Var</u>

868 a Precursor emissions in the Rest Of the World (ROW) other than CHN, KOR, and JPN

869 b Each factor was fixed at the year 1980 level

870 c CH₄ concentration increased until 2000 and flattened thereafter

871 d ~~InterAnnual-Temporal~~ Variation (~~IAV~~Var) of each factor was considered

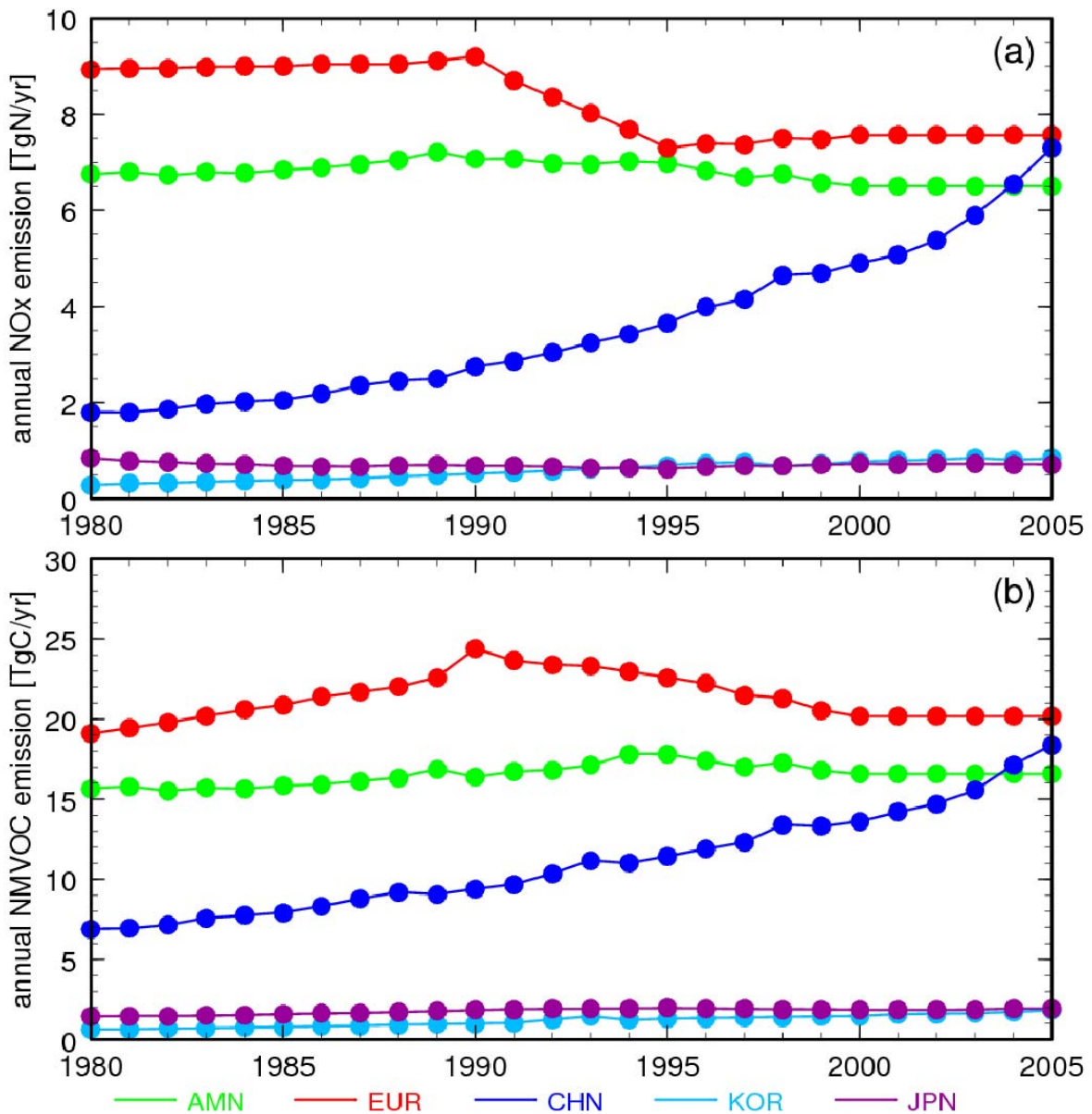


872

873 **Figure 1.** Linear trends of (a) NO_x and (b) NMVOC emission during the simulation period

874 (1980–2005) used in the study. Significant trends at 5 % risk level are colored. Source regions

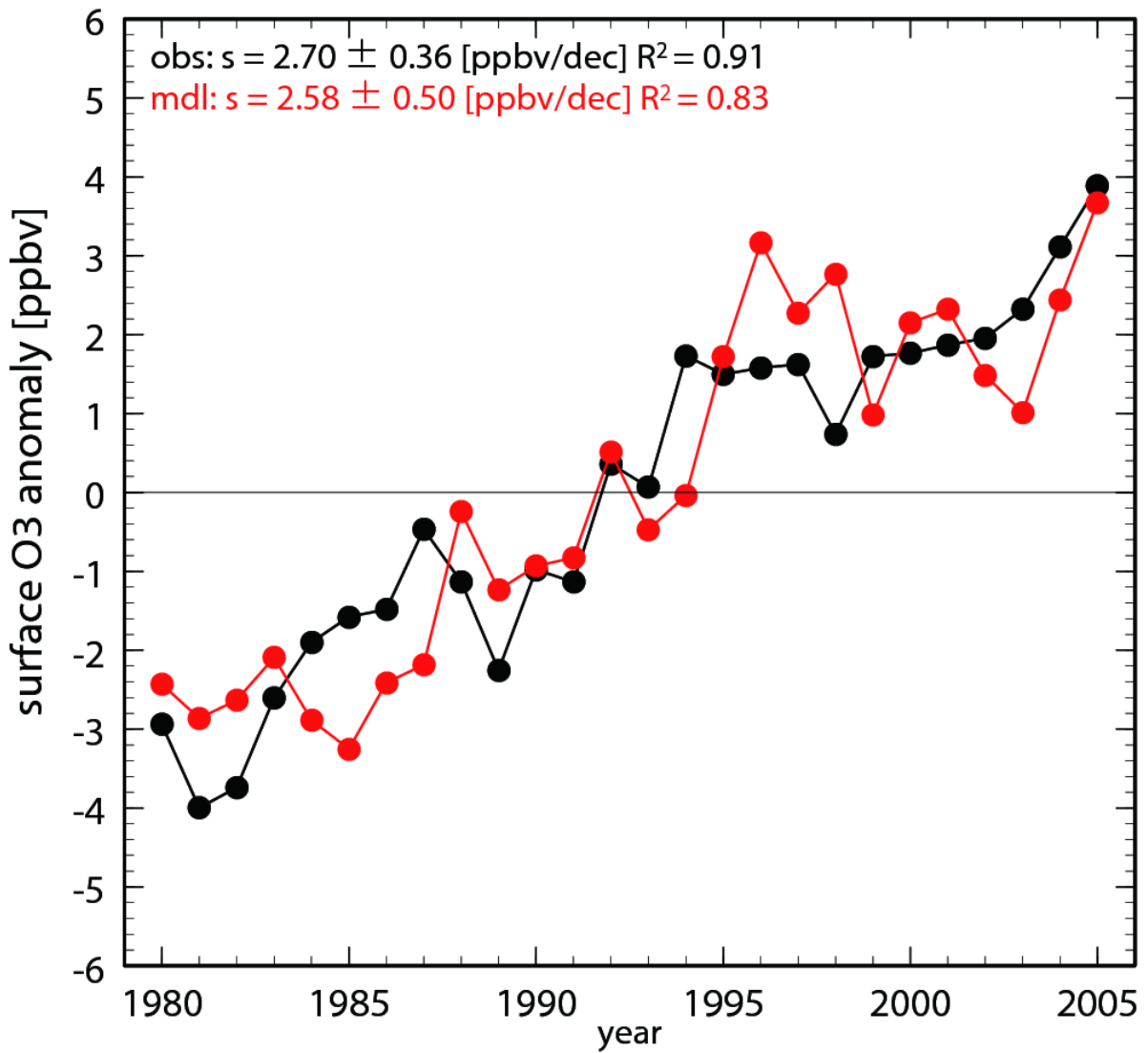
875 for tracer tagging are also displayed in the top figure.



876

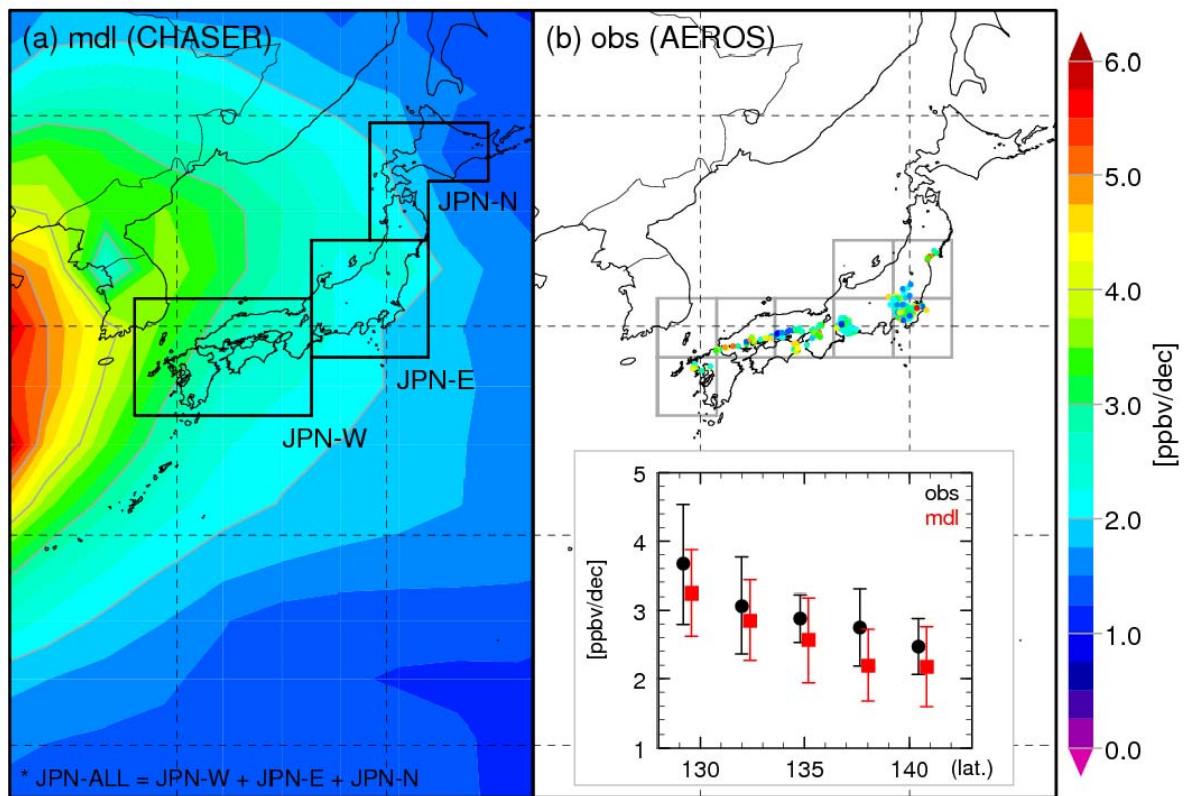
877 **Figure 2.** Temporal evolution of emissions of (a) NO_x and (b) NMVOC averaged over several

878 source areas in the Northern Hemisphere depicted in Fig. 1.



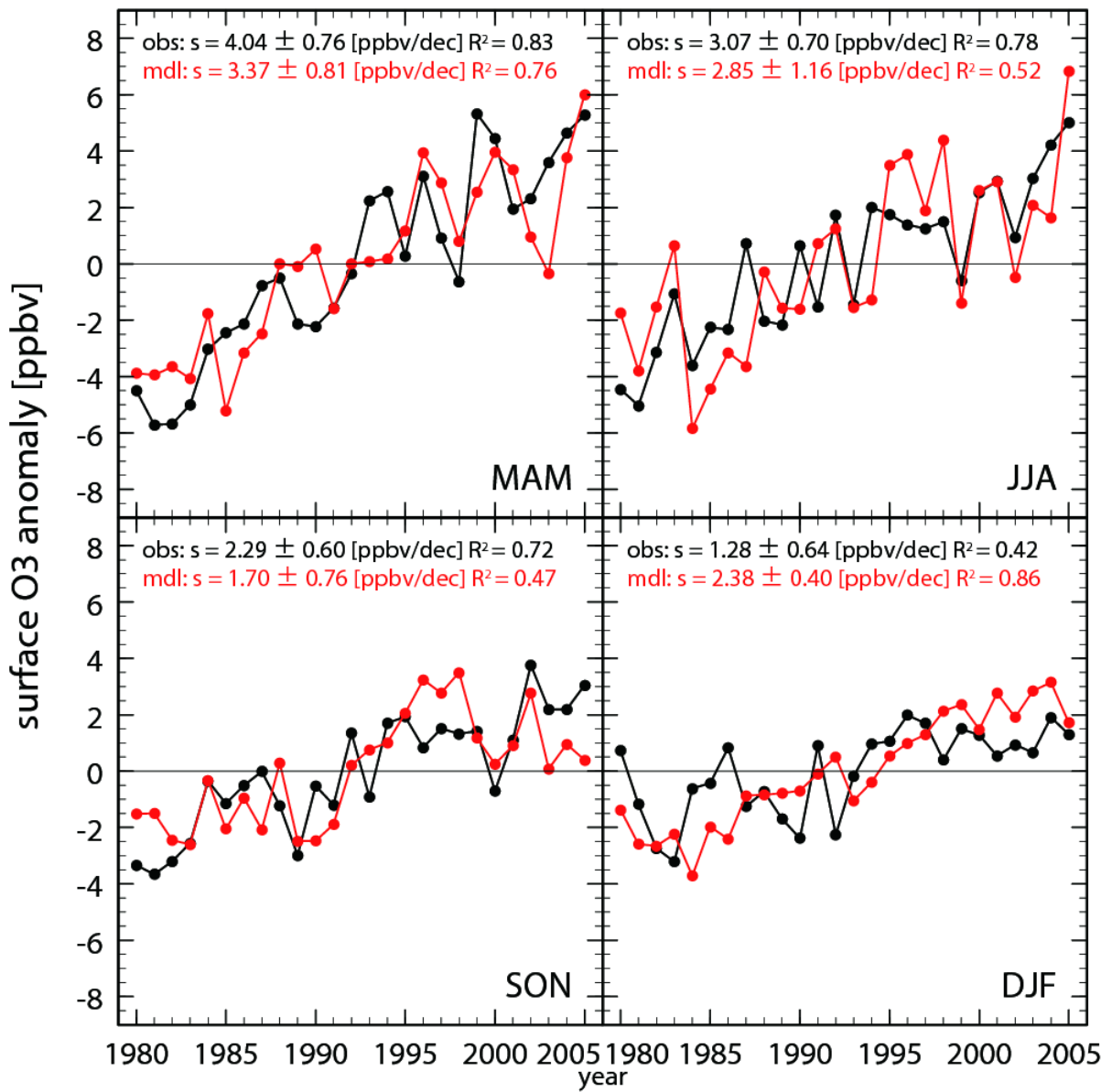
879

880 **Figure 3.** The temporal changes of annual mean surface O₃ anomaly averaged over Japan
 881 from observation (AEROS: black) and model calculation (red). Anomalies are defined as
 882 deviations from the values averaged over 1980–2005. The slope of a regression (s) for 1980–
 883 2005 with their 95 % confidence interval and R² are also shown.



884

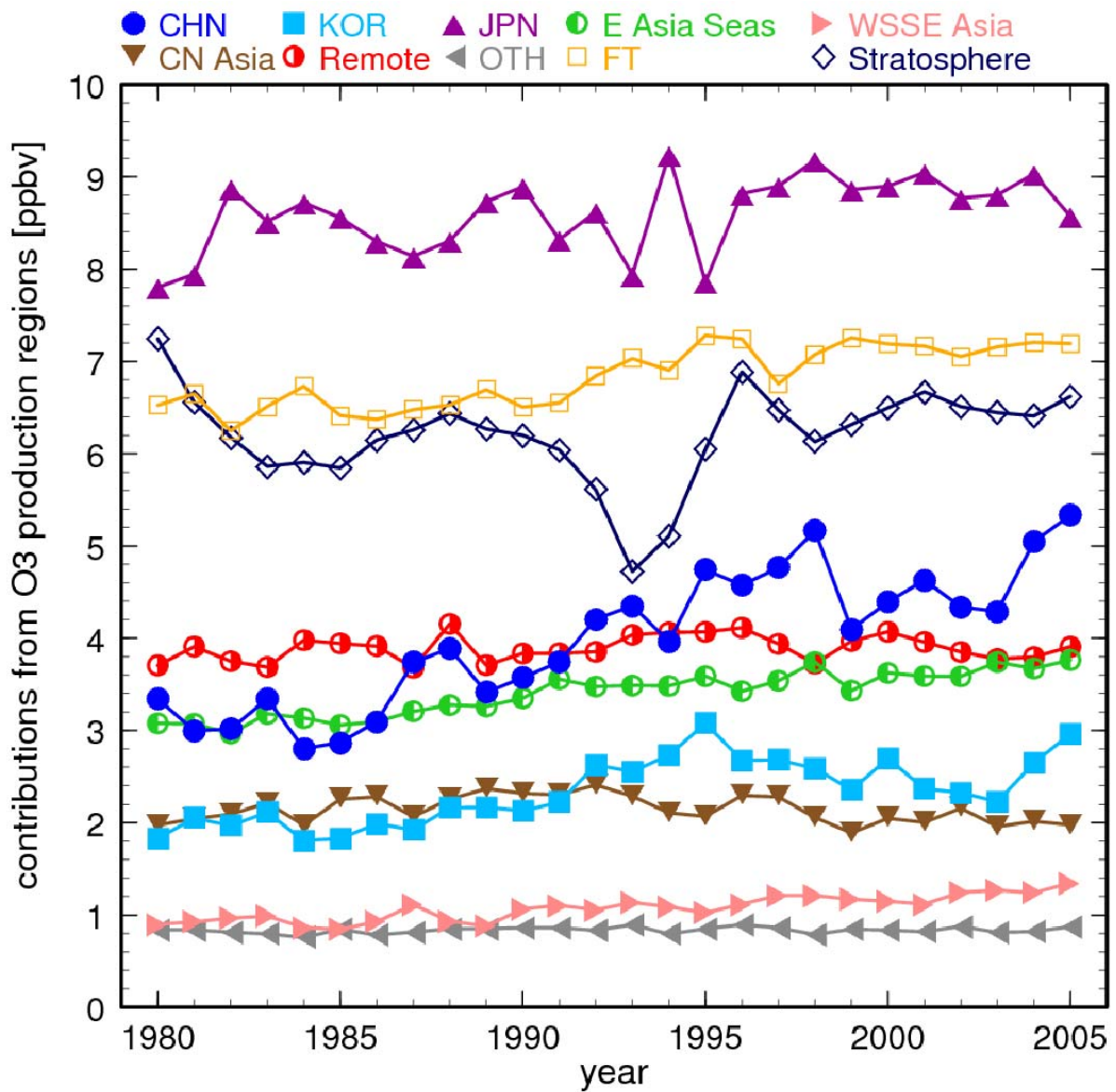
885 **Figure 4.** The linear trend of annual mean surface O₃ in 1980–2005 calculated from (a) model
 886 simulations and (b) observations at AEROS monitoring sites. The inset in figure (b) shows the
 887 longitudinal change of linear trends (black: AEROS observation; red: model) averaged within
 888 the model grids shown by gray rectangles. The error bars denote their 95 % confidence
 889 intervals. The black-rimmed areas in figure (a) are the area for averaging used in the figures
 890 from Fig. 6. Note that JPN-ALL is the sum of JPN-W, JPN-E, and JPN-N areas and used for
 891 the averaging in those figures.



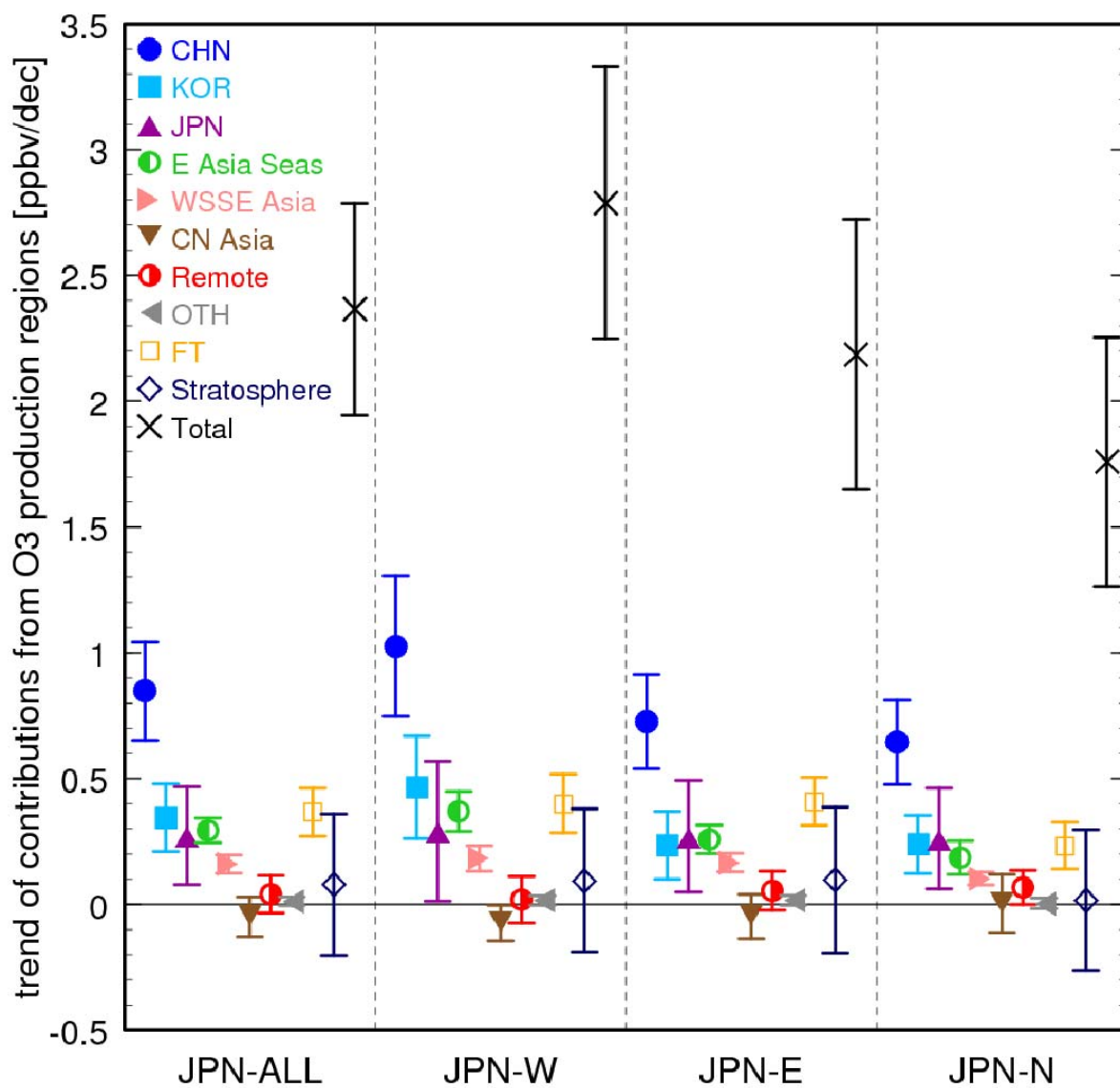
892

893 **Figure 5.** Same as Fig. 3 but the temporal changes of seasonal mean surface O₃ anomaly

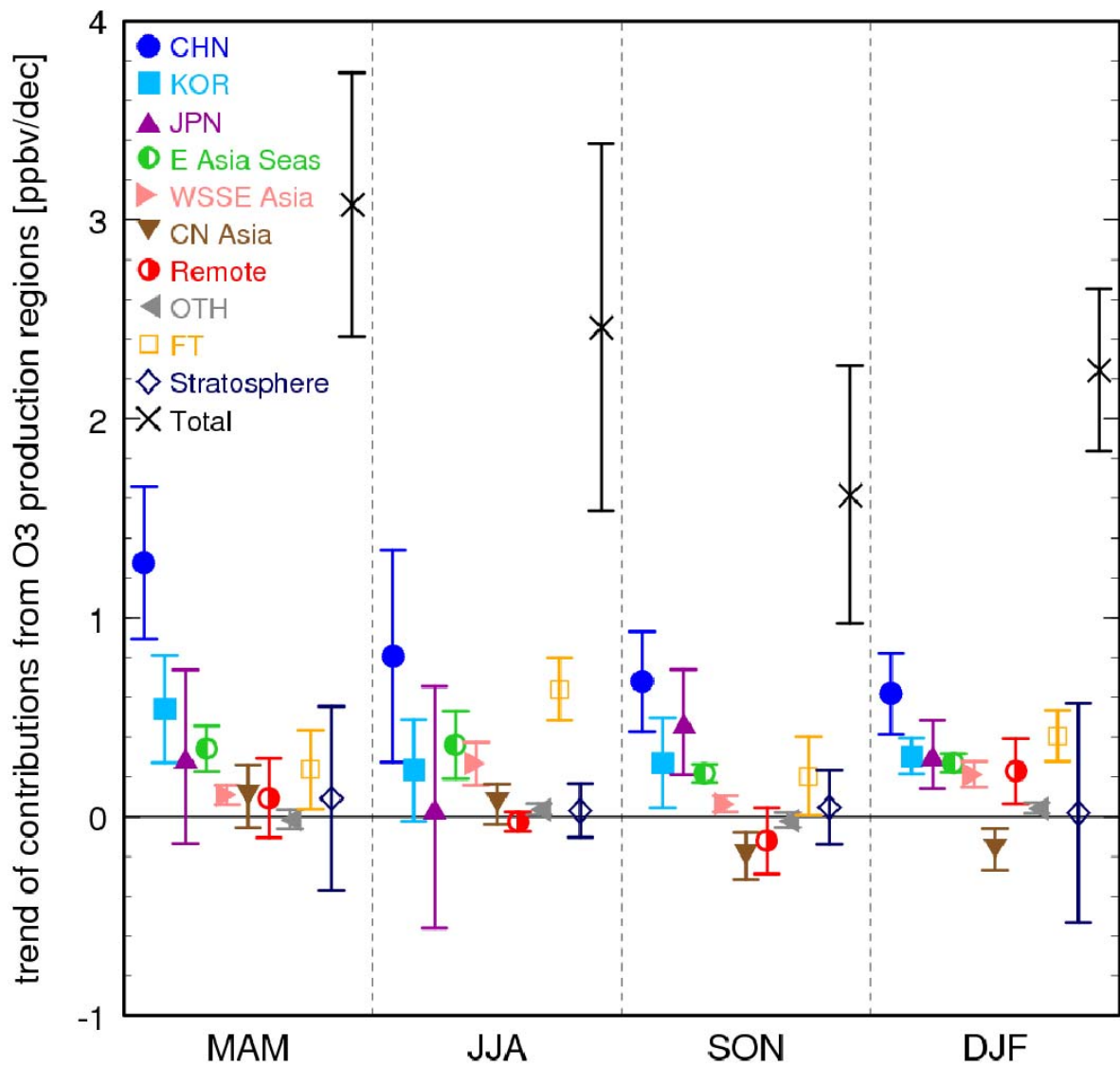
894 averaged over Japan from observations (AEROS: black) and model calculations (red).



895
 896 **Figure 6.** Long-term changes of annual mean contributions from source regions to surface O₃
 897 over Japan. Some source regions are grouped: E-Asia-Seas is the sum of NPC, JPS, and ECS;
 898 WSSE Asia is the sum of MES, IND, IDN, and IDC; CN Asia is the sum of CAS and ESB;
 899 Remote is the sum of AMN, NAT, and EUR; and OTH is the other regions in the planetary
 900 boundary layer.

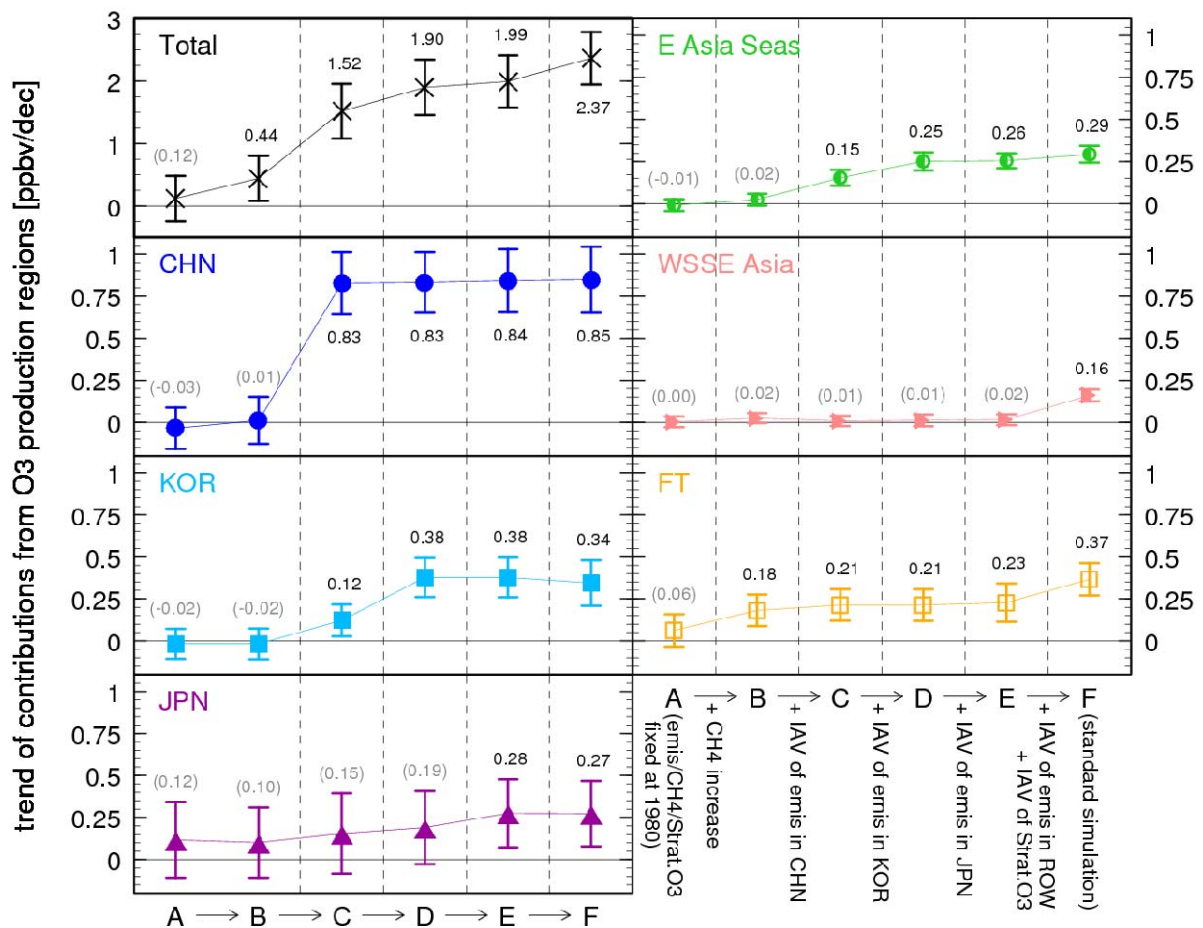


901
 902 **Figure 7.** Linear trends of annual mean contributions in 1980–2005 from source regions to
 903 surface O₃ over Japan shown in Fig. 6 (JPN-ALL) and those averaged in three sub-regions in
 904 Japan (JPN-W, JPN-E, and JPN-N). Error bars are 95 % confidence intervals.



905

906 **Figure 8.** Linear trends of the contributions in 1980–2005 from source regions to surface O₃
 907 over Japan in different seasons: spring (MAM), summer (JJA), fall (SON), and winter (DJF).
 908 Error bars are 95 % confidence intervals.



909

910 **Figure 9.** Linear trends of the annual mean contributions in 1980–2005 from source regions
 911 to surface O₃ over Japan in the sensitivity simulations and the standard simulation (error bars
 912 are 95 % confidence intervals). The exact values of the trends are also shown in the figure; the
 913 trends without sufficient statistical significance are shown in parentheses. The trends of each
 914 region’s contribution in the simulations A–E and F (the standard simulation) are arranged
 915 from left to right in each panel.